Energy Conversion and Management 127 (2016) 443–460

Contents lists available at ScienceDirect

Energy Conversion and Management

journal homepage: www.elsevier.com/locate/enconman

Lambert W-function based exact representation for double diode model of solar cells: Comparison on fitness and parameter extraction

Xiankun Gao, Yan Cui *, Jianjun Hu, Guangyin Xu, Yongchang Yu

Key Laboratory of New Materials and Facilities for Rural Renewable Energy, Ministry of Agriculture, Henan Agricultural University, Zhengzhou 450002, China

ARTICLE INFO

Article history:
Received 24 June 2016
Received in revised form 23 August 2016
Accepted 2 September 2016
Available online 15 September 2016

Keywords:
Solar cell
Double diode model
Lambert W-function
Parameter extraction

ABSTRACT

Accurate modeling and parameter extraction of solar cells play an important role in the simulation and optimization of PV systems. This paper presents a Lambert *W*-function based exact representation (LBER) for traditional double diode model (DDM) of solar cells, and then compares their fitness and parameter extraction performance. Unlike existing works, the proposed LBER is rigorously derived from DDM, and in LBER the coefficients of Lambert *W*-function are not extra parameters to be extracted or arbitrary scalars but the vectors of terminal voltage and current of solar cells. The fitness difference between LBER and DDM is objectively validated by the reported parameter values and experimental *I–V* data of a solar cell and four solar modules from different technologies. The comparison results indicate that under the same parameter values, the proposed LBER can better represent the *I–V* and *P–V* characteristics of solar cells and provide a closer representation to actual maximum power points of all module types. Two different algorithms are used to compare the parameter extraction performance of LBER and DDM. One is our restart-based bound constrained Nelder-Mead (rbcNM) algorithm implemented in Matlab, and the other is the reported R_{cr}-IJADE algorithm executed in Visual Studio. The comparison results reveal that, the parameter values extracted from LBER using two algorithms are always more accurate and robust than those from DDM despite more time consuming. As an improved version of DDM, the proposed LBER is quite promising for PV simulation and thus deserves serious attention.

1. Introduction

Ever since solar cell came on the scene, accurate modeling and parameter extraction of its nonlinear *I–V* (current vs. voltage) characteristics have drawn considerable attention as a useful tool for further simulation, evaluation, control and maximum energy harvesting of photovoltaic (PV) systems. Despite numerous models have been developed during the past decades to simulate the behavior of solar cells, only two lumped parameter equivalent circuit models are used practically: single diode model (SDM) and double diode model (DDM) [1–3]. In the equivalent circuit of DDM illustrated by Fig. 1(a), the solar cell under illumination is modeled as a photocurrent source connected with two exponential-type ideal diodes and two parasitic resistors. Diode D_1 simulates the diffusion process of the minority carriers into the depletion layer, while D_2 represents the carrier recombination in the space charge region of the junction [4]. Correspondingly, I_{D1} and I_{D2} stand for diffusion and recombination current components respectively, which are usually expressed by Shockley equation. As depicted in Fig. 1(b), SDM is developed by combining both diode currents together with the introduction of a non-physical diode ideality factor. From this point of view, SDM is a simplified version of DDM.

For a given irradiance and temperature, the *I–V* relationship in Fig. 1(a) and (b) can be represented respectively by the following DDM Eq. (1) and SDM Eq. (2).

$$I = I_{ph} - I_{01}\left[\exp\left(\frac{V+IR_s}{n_1V_{th}}\right)-1\right] - I_{02}\left[\exp\left(\frac{V+IR_s}{n_2V_{th}}\right)-1\right] - \frac{V+IR_s}{R_{sh}} \tag{1}$$

$$I = I_{ph} - I_0\left[\exp\left(\frac{V+IR_s}{nV_{th}}\right)-1\right] - \frac{V+IR_s}{R_{sh}} \tag{2}$$

where I, V, I_{ph}, I_{01}, I_{02}, I_0, n_1, n_2, n, R_s, and R_{sh} are the terminal current, terminal voltage, photocurrent, diode saturation currents, diode ideality factors, series resistance, and shunt resistance, respectively. Thermal voltage $V_{th} = N_skT/q$, where N_s is the number of cells in ser-

* Corresponding author.
E-mail addresses: gaoxiankun78@163.com (X. Gao), cuiyan6198@163.com (Y. Cui), hujianjun@163.com (J. Hu), xgy4175@126.com (G. Xu), hnyych@163.com (Y. Yu).

http://dx.doi.org/10.1016/j.enconman.2016.09.005
0196-8904/

Nomenclature

bcNM	bound constrained Nelder-Mead algorithm
ACE	absolute current error (A)
ACE_{cal}	absolute current error of calculated current (A)
ACE_{sim}	absolute current error of simulated current (A)
DDM	double diode model
EESDM	exact explicit single diode model
fval	RMSE_{cal} obtained by the *S*th run of bcNM
$f_M(V, I, X)$	error function
G	irradiance
I	terminal current (A)
I_0, I_{01}, I_{02}	diode reverse saturation currents (A)
$I_{0\min}$, $I_{0\max}$	lower and upper bounds on $I_{01,2}$ (A)
I_{cal}	calculated current (A)
I_D, I_{D1}, I_{D2}	diode currents (A)
I_{ph}	photocurrent (A)
I_{sc}	short-circuit current (A)
I_{sim}	simulated current (A)
k	Boltzmann constant ($1.3806503 \times 10^{-23}$ J/K)
LB	lower bound on $\boldsymbol{X}$
LBER	Lambert *W*-function based exact representation
m	parameter dimension
Max_NFEs	maximum number of function evaluations
MaxIter	maximum number of iterations
MaxFunEvals	maximum number of function evaluations
MPP	maximum power point
n, n_1, n_2	diode ideality factors
N	number of the experimental *I*–*V* data
N_s	number of cells in series
NM	Nelder-Mead algorithm
ObjFun	objective function
plotFcns	plot function
q	electronic charge (1.60217646 × 10−19 C)
r	ratio of diffusion current to the sum ofdiffusion and recombination currents
r_i	ith element of r
R_s	series resistance (Ω)
R_{sh}	shunt resistance (Ω)
RMSE_{cal}	root mean square error of calculated current
RMSE_{sim}	root mean square error of simulated current
S	restarting number of bcNM
SDM	single diode model
T	cell temperature (K)
TolFun	termination tolerance on RMSEcal (X)
TolFun_runs	RMSEcal difference
TolX	termination tolerance on X
UB	upper bound on X
V	terminal voltage (V)
V_{oc}	open-circuit voltage (V)
V_{th}	thermal voltage (V)
W_0	principal branch of Lambert W-function
X	parameter vector
X_0	initial value of X
μ	population size

ies, k is the Boltzmann constant, q is the electronic charge, and T is the absolute temperature in Kelvin and can be calculated by 273.15 plus the cell temperature in Celsius.

As can be seen from Eqs. (1) and (2), there are seven parameters (I_{ph}, I_{01}, I_{02}, n_1, n_2, R_s and R_{sh}) in DDM and five parameters (I_{ph}, I_0, n, R_s and R_{sh}) in SDM need to be extracted. The knowledge of these parameters is used not only to evaluate the performance and improve the design, fabrication process and quality control of solar cells, but also to extract the maximum power point (MPP) of PV array [5–9]. Hence, it is imperative to accurately extract these parameters from the experimental *I*–*V* data of solar cells. Unfortunately, both DDM Eq. (1) and SDM Eq. (2) are implicit nonlinear transcendental equations, mainly because neither the current I nor the voltage V can be explicitly expressed only by using elementary functions. This inherent implicit nature increases the complexity and difficulty not only of parameter extraction but also of simulation of PV systems [10], and thus calls for explicit expressions for DDM Eq. (1) and SDM Eq. (2) prior to their parameter extraction phase.

Thanks to Lambert *W*-function [11], which makes it possible for transforming implicit SDM Eq. (2) into the exact explicit single diode model (EESDM) Eq. (3) [12].

$$I = \frac{R_{sh}(I_{ph} + I_0) - V}{R_s + R_{sh}} - \frac{nV_{th}}{R_s} W_0(\alpha) \tag{3}$$

where W_0 is the principal branch of Lambert *W*-function, and

$$\alpha = \frac{I_0 R_s R_{sh}}{nV_{th}(R_s + R_{sh})} \exp\left[\frac{R_{sh}(R_s I_{ph} + R_s I_0 + V)}{nV_{th}(R_s + R_{sh})}\right] \tag{4}$$

The most desirable feature of EESDM Eq. (3) is that for any value of voltage V the corresponding exact value of current I can be calculated straightforwardly, which enables more accurate *I*–*V* characteristics [13–16], MPP tracking [17–19], optimum load [20–22] and efficient model parameter extraction [23–28]. A recent comparative study [29] revealed that Lambert *W*-function based analytical method [10] presents fewer errors in comparison to iterative method [30]. One of our previous studies [31] shown that EESDM Eq. (3) is much more accurate and reliable than SDM Eq. (2) in parameter extraction of solar cells. In general, EESDM Eq. (3) has better accuracy, applicability, and convergence than SDM Eq. (2) though the calculation speed is relatively lower [32].

Inspired by the superiority of EESDM Eq. (3), two Lambert *W*-function based explicit expressions have been developed in an attempt to approximate DDM Eq. (1). Authors in Ref. [33] reported an explicit double exponential model as an alternative to DDM. Unfortunately, this alternative model is only an approximation to DDM, since they are not exactly analogous for all possible arbitrary sets of parameters [33]. The validation results in Ref. [34] show that the equivalence between the alternative model and DDM

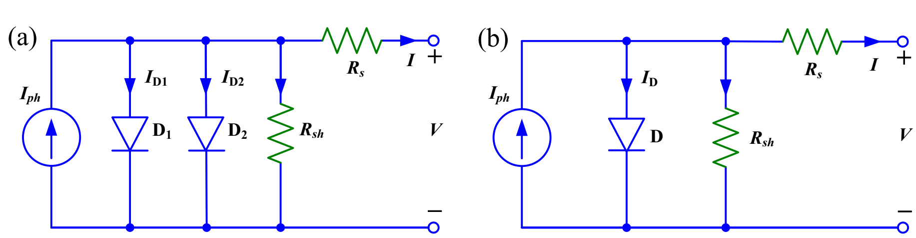

Fig. 1. Equivalent circuits of a solar cell under illumination: (a) double diode model (DDM), and (b) single diode model (SDM).

can only come into existence when introducing equivalent resistive losses with appropriate coefficients. Moreover, comparing with DDM Eq. (1), this alternative model has two extra parameters to be extracted, which makes model parameter extraction even more difficult. Based on DDM Eq. (1), Ref. [35] proposed an new explicit double-diode modeling method based on Lambert W-function. Regrettably, the explicit current equation in Ref. [35] is derived under the presupposition of $n_1 = n_2$, as evidenced by the derivation and extracted parameter values reported therein. It should be noted that this presupposition is arbitrary and contradictory to the parameter extraction results of most solar cells [36–42]. If $n_1 = n_2$ is true, then the explicit current equation in Ref. [35] essentially is a special EESDM equation rather than a exact explicit expression of DDM Eq. (1). To sum up, both the two existing explicit expressions are only approximations and have low fidelity to DDM Eq. (1). In this context, it is necessary to develop an exact representation for DDM Eq. (1) using Lambert W-function. However, to the best of our knowledge there is no relevant report in the literature, which can be attributed to DDM Eq. (1) contains two exponential terms and has more parameters than SDM Eq. (2).

In light of the preceding discussion, the main objective of this paper is to propose a Lambert W-function based exact representation (LBER) for DDM Eq. (1). The proposed LBER is derived without any approximation and any hypothesis, and only contains model parameters I_{ph}, I_{01}, I_{02}, n_1, n_2, R_s and R_{sh}. Unlike existing works, in the proposed LBER the coefficients of Lambert W-function are not extra parameters to be extracted or arbitrary scalars but the vectors of terminal voltage and current of solar cells. Moreover, the proposed LBER is quite general, since it is rigorously derived from DDM Eq. (1) and should therefore hold for various solar cells. The presentation above is exactly the novelty of this paper too. To validate the accuracy of the proposed LBER, the second contribution of this paper is to verify the fitness difference between LBER and DDM. It is designed to investigate under the same parameter values, which one of them can better represent the I–V and P–V (power vs. voltage) characteristics of solar cells. The fitness comparison between LBER and DDM is carried out using the reported parameter values and experimental I–V data of five types of solar cells: 57 mm diameter commercial (R.T.C. France) silicon solar cell [43], mono-crystalline (SM55) module [44], multi-crystalline (KC200GT) module [45], thin-film (ST40) module [46] and amorphous silicon triple junction module [47]. Another contribution of this paper is to compare the parameter extraction performance of LBER and DDM. It aims to reveal under the same simulation conditions, which one of them can extract more accurate parameter values. To provide a comprehensive comparison, two different algorithms are employed for parameter extraction of LBER and DDM. One is our restart-based bound constrained Nelder-Mead (rbcNM) algorithm [31] implemented in Matlab, and the other is the reported R_{cr}-IJADE algorithm [48] executed in Visual Studio.

The rest of this paper is organized as follows. Section 2 devotes to deriving the proposed LBER from DDM Eq. (1). Section 3 focuses on fitness comparison between DDM and LBER. Section 4 describes the rbcNM algorithm [31] and revises it for parameter extraction of DDM and LBER. Section 5 elaborates and compares the parameter extraction results of LBER and DDM, and finally, Section 6 concludes this paper.

2. Lambert *W*-function based exact representation (LBER)

The biggest obstacle to get the Lambert W-function based exact representation of DDM Eq. (1) is the presence of two exponential terms. Although these two exponential terms are potentially relevant, they can be addressed separately so as to evaluate their respective contribution under different terminal voltage and current of solar cells.

2.1. Derivation of the proposed LBER

To separate one exponential term from the other, a real vector r is defined below to denote the ratio of diffusion current to the sum of diffusion and recombination currents.

$$r = \frac{I_{01}\left[\exp\left(\frac{V+IR_s}{n_1V_{th}}\right)-1\right]}{I_{01}\left[\exp\left(\frac{V+IR_s}{n_1V_{th}}\right)-1\right]+I_{02}\left[\exp\left(\frac{V+IR_s}{n_2V_{th}}\right)-1\right]} \tag{5}$$

where r is N-vector, N is the number of the experimental I–V data, and the ith element r_i can be computed from each pair of experimental I–V data when knowing the parameter values of I_{01}, I_{02}, n_1, n_2 and R_s. Clearly, the value of r_i varies with terminal voltage V and current I, and can be confined in the interval $r_i \in (0,1)$.

After some algebraic manipulations and using r, DDM Eq. (1) can be split into a sum of Eqs. (6) and (7).

$$I = I_{ph} - \frac{I_{01}}{r}\left[\exp\left(\frac{V+IR_s}{n_1V_{th}}\right)-1\right] - \frac{V+IR_s}{R_{sh}} \tag{6}$$

$$I = I_{ph} - \left(\frac{I_{02}}{1-r}\right)\left[\exp\left(\frac{V+IR_s}{n_2V_{th}}\right)-1\right] - \frac{V+IR_s}{R_{sh}} \tag{7}$$

Apparently, Eqs. (6) and (7) are described by linear and single-exponential functions, each of which could be seen as a particular SDM equation. That is, DDM Eq. (1) can be treated as the composition of two particular SDM equations. Similar to transforming SDM Eq. (2) into EESDM Eq. (3), the exact explicit representation for Eqs. (6) and (7) can be expressed using Lambert W-function as follows

$$I = \frac{R_{sh}(I_{ph}+I_{01}/r)-V}{R_s+R_{sh}} - \frac{n_1V_{th}}{R_s}W_0(\theta_1) \tag{8}$$

$$I = \frac{R_{sh}[I_{ph}+I_{02}/(1-r)]-V}{R_s+R_{sh}} - \frac{n_2V_{th}}{R_s}W_0(\theta_2) \tag{9}$$

where

$$\theta_1 = \frac{I_{01}R_sR_{sh}}{rn_1V_{th}(R_s+R_{sh})}\exp\left[\frac{R_{sh}(R_sI_{ph}+R_sI_{01}/r+V)}{n_1V_{th}(R_s+R_{sh})}\right] \tag{10}$$

$$\theta_2 = \frac{I_{02}R_sR_{sh}}{(1-r)n_2V_{th}(R_s+R_{sh})}\exp\left[\frac{R_{sh}[R_sI_{ph}+R_sI_{02}/(1-r)+V]}{n_2V_{th}(R_s+R_{sh})}\right] \tag{11}$$

Left-multiplying Eq. (8) by r, Eq. (9) by $(1-r)$, and add them termwise, we get the Lambert W-function based exact representation (LBER)

$$I = \frac{R_{sh}(I_{ph}+I_{01}+I_{02})-V}{R_s+R_{sh}} - r\frac{n_1V_{th}}{R_s}W_0(\theta_1) - (1-r)\frac{n_2V_{th}}{R_s}W_0(\theta_2) \tag{12}$$

2.2. Differences among LBER, DDM and existing works

The proposed LBER Eq. (12) is closely linked with but different from DDM Eq. (1). Since r is determined by Eq. (5), the proposed LBER Eq. (12) has seven identical parameters as those included in DDM Eq. (1), and both of them are implicit equations. But on the other hand, the proposed LBER Eq. (12) is expressed by Lambert W-function and calculated by means of series expansion, asymptotic approximation and Padé approximant [11], whereas DDM Eq. (1) is expressed and calculated only by elementary function. In addition, it is worth mentioning that if r is the null vector, the unitary vector, or $n_1 = n_2$, the proposed LBER Eq. (12) will degenerate into EESDM Eq. (3) (see Table 10 for an example).

It is also important to clarify the difference between the proposed LBER Eq. (12) and the existing works. Since the double diodes in Ref. [33] and those in Fig. 1(a) are connected in different ways, the diode parameters in Ref. [33] have different physical sense from those in DDM Eq. (1) and LBER Eq. (12). Besides, the alternative model in Ref. [33] has nine parameters to be extracted, whereas the proposed LBER Eq. (12) contains only seven. Most important of all, the two extra parameters in Ref. [33] are undetermined scalars, while in the proposed LBER r and $(1 - r)$ are real vectors and can be computed by Eq. (5), which is the biggest difference between them. As for the relationship between LBER Eq. (12) and the explicit current equation in Ref. [35], by termwise comparison it can be found that the former degenerates into the latter when $r_i = 0.5$ and $I_{01} = I_{02}$. From this point of view, the latter can be viewed as a special case of the former. For these reasons, this paper only covers the comparison between DDM Eq. (1) and the proposed LBER Eq. (12), which are denoted as DDM and LBER in the following illustrations and tables, respectively.

3. Fitness comparison between LBER and DDM

Theoretically, the proposed LBER Eq. (12) is rigorously derived from DDM Eq. (1), the performance of them should be the same. But in fact, due to the intervention of Lambert *W*-function or not, they are expressed and calculated in different ways and hence have different fitness to experimental *I–V* data of solar cells. The reason to compare the fitness of LBER and DDM is mainly because it exerts significant influence on the accuracy of numerical parameter extraction.

3.1. Fitness criterion

Before proceeding to evaluate the fitness of DDM and LBER under the same condition, a fitness criterion should be first defined. Substituting the experimental *I–V* data and parameter values of I_{ph}, I_{01}, I_{02}, n_1, n_2, R_s and R_{sh} into the right side of Eqs. (1) and (12), the calculated currents of DDM and LBER can be given respectively by

$$I_{cal\_DDM} = I_{ph} - I_{01}\left[\exp\left(\frac{V+IR_s}{n_1V_{th}}\right)-1\right] - I_{02}\left[\exp\left(\frac{V+IR_s}{n_2V_{th}}\right)-1\right] - \frac{V+IR_s}{R_{sh}} \tag{13}$$

$$I_{cal\_LBER} = \frac{R_{sh}(I_{ph}+I_{01}+I_{02})-V}{R_s+R_{sh}} - r\frac{n_1V_{th}}{R_s}W_0(\theta_1) - (1-r)\frac{n_2V_{th}}{R_s}W_0(\theta_2) \tag{14}$$

Absolute current error (ACE) between the calculated and experimental currents can be expressed respectively as

$$ACE_{cal\_DDM} = |I_{cal\_DDM} - I| \tag{15}$$

$$ACE_{cal\_LBER} = |I_{cal\_LBER} - I| \tag{16}$$

Similar to Refs. [48–60], the root mean square error (RMSE) between the calculated and experimental currents is used as the criteria to quantify the fitness of DDM and LBER, which can be represented respectively as

$$\mathrm{RMSE}_{cal\_DDM} = \sqrt{\frac{1}{N}\sum_{i=1}^{N}(I_{cal\_DDM} - I)^2} \tag{17}$$

$$\mathrm{RMSE}_{cal\_LBER} = \sqrt{\frac{1}{N}\sum_{i=1}^{N}(I_{cal\_LBER} - I)^2} \tag{18}$$

Clearly, under the same parameter values of I_{ph}, I_{01}, I_{02}, n_1, n_2, R_s and R_{sh}, the lower the value of RMSE_{cal}, the better the fitness to the experimental *I–V* data of solar cells.

3.2. Fitness comparison results

To ensure an objective and fair fitness comparison between DDM and LBER, the reported parameter values and experimental *I–V* data of a solar cell and four types of solar modules are preferentially considered in this subsection.

3.2.1. Results for solar cell

For solar cell case, the experimental *I–V* data of a 57 mm diameter commercial (R.T.C. France) silicon solar cell [43] together with the parameter values listed in Table 1 are substituted into Eqs. (13)–(18) to quantify the fitness of DDM and LBER. The experimental *I–V* data has been adopted from the system under 1000 W/m^2 at 33 °C and utilized by several algorithms for parameter extraction of DDM Eq. (1). As shown in Table 1, the parameter values extracted from this set of experimental *I–V* data are originally published in Refs. [48–62] and named after their respective algorithms.

The last two columns of Table 1 summarize the RMSE_{cal} values of DDM and LBER of R.T.C. France solar cell. It is evident that all the RMSE_{cal_LBER} values are remarkably lower than those of RMSE_{cal_DDM}, which reveals that the proposed LBER outperforms DDM in representing the experimental *I–V* data of solar cell. Moreover, it is interesting to observe from Table 1 that the more accurate the parameter values, the less the difference between RMSE_{cal_DDM} and RMSE_{cal_LBER}. It can be drawn that the fitness of DDM and LBER will tend to be the same once the real values of the model parameters are obtained.

Fig. 2(a) is a plot of the calculated and experimental currents versus voltage. As can be seen, the calculated current data of LBER makes different agreements with those of DDM, especially in the vicinity of open circuit voltage. To further illustrate this difference, Fig. 2(b) put into evidence the absolute current errors. It is clear that the absolute current errors of LBER are smaller than those of DDM over the entire range of experimental *I–V* data set. This confirms the proposed LBER can better represent experimental *I–V* data under the same parameter values of I_{ph}, I_{01}, I_{02}, n_1, n_2, R_s and R_{sh}. In addition, it is clear from Fig. 2(b) that the absolute current errors vary with terminal voltage. In low-voltage range (approximately below 0.4 V), the absolute current errors are very small and are almost the same for both LBER and DDM. But in high-voltage range, the absolute current errors increase with the increase of terminal voltage, and there is an obvious distinction between LBER and DDM. This indicates the superior fitness of the proposed LBER is mainly in high-voltage range.

3.2.2. Results for solar modules

For solar module case, the fitness difference between DDM and LBER is evaluated using the reported parameter values and experimental *I–V* data of four solar modules from different technologies: mono-crystalline (SM55) [44], multi-crystalline (KC200GT) [45], thin-film (ST40) [46] and amorphous silicon triple junction [47] types. The number of cells in series in these four solar modules are 36, 54, 42 [63] and 33 [47], respectively. The experimental *I–V* data of SM55 and KC200GT modules are extracted from the manufacturer's datasheets [44,45]. For comparing the degeneration of DDM Eq. (1) and the proposed LBER Eq. (12) in Section 5.2, the experimental *I–V* data of ST40 module are extracted from the *I–V* curves [46] generated by the commercial software PVsyst, which is based on standard one-diode-model [64]. The experimental *I–V* data of amorphous silicon triple junction module are collected in different measurement conditions [47]. The reported parameter values for these four solar modules are tabulated in Tables 2–5, respectively.

The last two columns of Tables 2–5 show the RMSE_{cal} values of DDM and LBER of the four solar modules at different levels of irradiance and temperature. It is obvious that all the RMSE_{cal_LBER}

Table 1
RMSE$_{cal}$ values of DDM and LBER calculated using the experimental I–V data of R.T.C. France solar cell [43] and the parameter values extracted by various algorithms.

Algorithms	I_{ph} (A)	I_{01} (μA)	I_{02} (μA)	n_1	n_2	R_s (Ω)	R_{sh} (Ω)	RMSE$_{cal_DDM}$	RMSE$_{cal_LBER}$
R$_{cr}$-IJADE [48]	0.760781	0.225974	0.749347	1.451017	2.00000	0.036740	55.485443	9.8249E−04	7.5778E−04
CSO [49]	0.76078	0.22732	0.72785	1.45151	1.99769	0.036737	55.3813	9.8253E−04	7.5794E−04
BMO [50]	0.76078	0.21110	0.87688	1.44533	1.99997	0.03682	55.8081	9.8266E−04	7.5497E−04
GOTLBO [51]	0.760752	0.800195	0.220462	1.999973	1.448974	0.036783	56.075304	9.8315E−04	7.5726E−04
ABSO [52]	0.76078	0.26713	0.38191	1.46512	1.98152	0.03657	54.6219	9.8360E−04	7.6559E−04
IGHS [53]	0.76079	0.97310	0.16791	1.92126	1.42814	0.03690	56.8368	9.8657E−04	7.5681E−04
TLBO [54]	0.76067	0.20289	0.29948	1.99809	1.47494	0.03646	55.8459	9.9272E−04	7.7900E−04
STLBO [54]	0.76078	0.22566	0.75217	1.45085	2.00000	0.03674	55.4920	9.9926E−04	7.6502E−04
BBO-M [55]	0.76083	0.59115	0.24523	2.00000	1.45798	0.03664	55.0494	1.0504E−03	7.9530E−04
GGHS [53]	0.76056	0.37014	0.13504	1.49638	1.92998	0.03562	62.7899	1.0684E−03	8.7799E−04
DE [55]	0.76079	0.36605	0.26320	1.91164	1.46500	0.03661	56.0213	1.0698E−03	8.1017E−04
FPA [56]	0.760795	0.300088	0.166159	1.47477	2.0000	0.0363342	52.3475	1.2424E−03	8.8949E−04
HS [53]	0.76176	0.12545	0.25470	1.49439	1.49989	0.03545	46.82696	1.2597E−03	1.0538E−03
MPCOA [57]	0.76078	0.31259	0.04528	1.47844	1.78549	0.03635	54.2531	2.3115E−03	1.4674E−03
CARO [58]	0.76075	0.29315	0.09098	1.47338	1.77321	0.03641	54.3967	2.3227E−03	1.4688E−03
ABC [59]	0.7608	0.0407	0.2847	1.4495	1.4885	0.0364	53.7804	2.4989E−03	1.5756E−03
BBO [55]	0.75940	0.95830	0.14885	1.85714	1.42309	0.03673	58.4585	3.3466E−03	2.1749E−03
DE [60]	0.76078	0.22599	0.75438	1.44972	1.99999	0.03674	55.4922	4.8520E−03	2.9027E−03
ABSO [60]	0.76078	0.22599	0.75439	1.44972	1.99999	0.03674	55.4922	4.8523E−03	2.9029E−03
ABCDE [60]	0.76078	0.22599	0.75437	1.44972	1.99998	0.03674	55.4921	4.8528E−03	2.9032E−03
MPSO [60]	0.76078	0.22614	0.75097	1.44978	1.99927	0.03674	55.4860	4.8560E−03	2.9054E−03
PS [61]	0.7602	0.9889	0.0001	1.6000	1.1920	0.0320	81.3008	1.5177E−02	1.0028E−02
SA [62]	0.7623	0.4767	0.0100	1.5172	2.0000	0.0345	43.1034	1.6644E−02	1.0231E−02
PSO [59]	0.7623	0.4767	0.0100	1.5172	2.0000	0.0325	43.1034	1.7235E−02	1.0226E−02

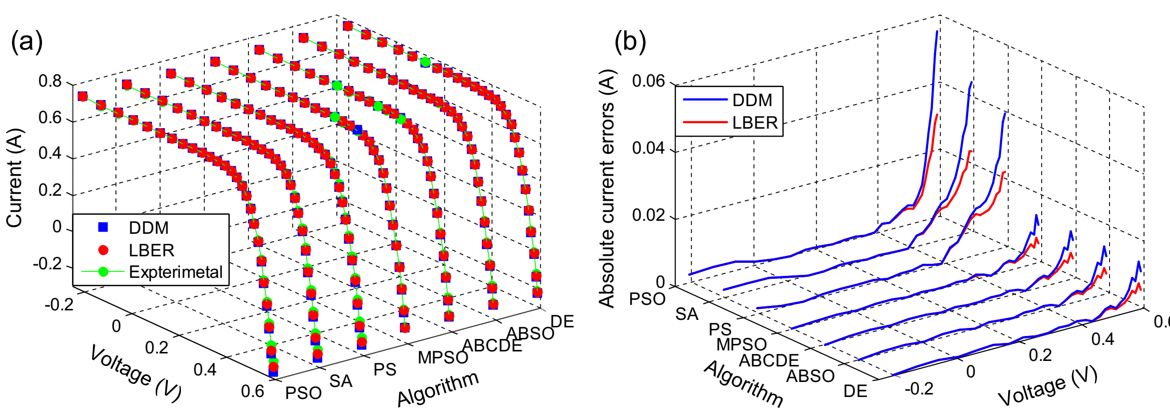

Fig. 2. Calculated curves of DDM and LBER using the experimental I–V data of R.T.C. France solar cell [43] and the parameter values extracted by several algorithms: (a) I–V characteristics, (b) absolute current errors.

Table 2
RMSE$_{cal}$ values of DDM and LBER calculated using the experimental I–V data of SM55 module [44] at different irradiance and temperature and the parameter values extracted by FPA [56].

Irrad. and temp.	I_{ph} (A)	I_{01} (μA)	I_{02} (μA)	n_1	n_2	R_s (Ω)	R_{sh} (Ω)	RMSE$_{cal_DDM}$	RMSE$_{cal_LBER}$
200 W/m^2, 25 °C	0.6905771	0.1398725	0.1419069	1.378175	3.45683	0.3390007	443.4634	2.7595E−02	2.4520E−02
400 W/m^2, 25 °C	1.380696	0.1392189	0.1215212	1.377924	2.297263	0.3386843	451.183	2.3406E−02	2.0073E−02
600 W/m^2, 25 °C	2.068947	0.1472423	0.1530210	1.382451	2.834106	0.3380305	480.1678	2.5406E−02	2.1550E−02
800 W/m^2, 25 °C	2.759354	0.1425452	0.6755132	1.379719	3.14591	0.3388229	469.336	6.0408E−02	4.2477E−02
1000 W/m^2, 25 °C	3.450253	0.1302402	0.359717	1.373022	2.114513	0.3392569	442.917	8.7788E−02	5.7704E−02
1000 W/m^2, 40 °C	3.467988	0.7258092	0.6681137	1.378014	3.896155	0.3389987	454.9449	4.4733E−02	2.7108E−02
1000 W/m^2, 60 °C	3.49099	5.24174	20.85424	1.378047	3.560465	0.338981	470.6224	2.9140E−02	2.0957E−02

Table 3
RMSE$_{cal}$ values of DDM and LBER calculated using the experimental I–V data of KC200GT module [45] at different irradiance and 25 °C and the parameter values extracted by FPA [56].

Irradiance	I_{ph} (A)	I_{01} (μA)	I_{02} (μA)	n_1	n_2	R_s (Ω)	R_{sh} (Ω)	RMSE$_{cal_DDM}$	RMSE$_{cal_LBER}$
200 W/m^2	1.651633	7.7421E−04	6.198045E−03	1.016906	2.492559	0.4076639	761.5569	1.3355E−01	9.0467E−02
400 W/m^2	3.295472	7.5326E−04	1.355235E−03	1.020557	2.687789	0.4009003	790.1216	9.2846E−02	7.4279E−02
600 W/m^2	4.939089	7.5720E−04	1.771260E−03	1.024232	2.752319	0.3959014	769.5941	2.2539E−01	1.1474E−01
800 W/m^2	6.577932	8.1733E−04	1.171566E−03	1.028472	2.615832	0.3827711	791.0941	2.9035E−01	1.5527E−01
1000 W/m^2	8.222643	7.8871E−04	3.345309E−03	1.030693	2.349279	0.3803971	790.3188	7.6007E−01	3.5855E−01

Table 4
$RMSE_{cal}$ values of DDM and LBER calculated using the experimental I–V data of ST40 module [46] at different irradiance and temperature and the parameter values extracted by FPA [56].

Irrad. and temp.	I_{ph} (A)	I_{01} (μA)	I_{02} (μA)	n_1	n_2	R_s (Ω)	R_{sh} (Ω)	$RMSE_{cal\_DDM}$	$RMSE_{cal\_LBER}$
200 W/m^2, 25 °C	0.5328492	1.28671	1.503562	1.484785	3.101258	1.140772	314.2327	2.4902E−02	2.3012E−02
400 W/m^2, 25 °C	1.071109	0.8122822	74.71976	1.438419	3.678599	1.147978	322.0261	1.3298E−02	1.1681E−02
600 W/m^2, 25 °C	1.606146	1.1969	47.38319	1.47787	3.60533	1.123132	339.4545	1.1314E−02	8.0224E−03
800 W/m^2, 25 °C	2.143522	1.035084	1.125682	1.462271	3.305267	1.138831	313.8327	1.8876E−02	9.4748E−03
1000 W/m^2, 25 °C	2.678046	1.19606	62.2786	1.477328	3.724013	1.121674	332.9976	2.4230E−02	1.0251E−02
1000 W/m^2, 40 °C	2.682986	4.657815	36.76408	1.457196	2.805913	1.135602	332.0241	1.4119E−01	5.8151E−02
1000 W/m^2, 55 °C	2.689642	19.78435	76.42367	1.457624	3.868232	1.138435	313.8128	2.6579E−01	1.0875E−01
1000 W/m^2, 70 °C	2.696194	67.20733	184.4388	1.447081	2.860334	1.141111	311.2677	4.0758E−01	1.6463E−01

Table 5
$RMSE_{cal}$ values of DDM and LBER calculated using the experimental I–V data in different measurement conditions and the parameter values of an amorphous silicon triple junction module with 11 cells connected in series [47].

Measurement conditions	I_{ph} (A)	I_{01} (A)	I_{02} (A)	n_1	n_2	R_s (Ω)	R_{sh} (Ω)	$RMSE_{cal\_DDM}$	$RMSE_{cal\_LBER}$
893 W/m^2, 40.2 °C	1.986	3.864E−11	8.913E−05	1	2.69	1.052	121	2.6388E−02	1.6336E−02
788 W/m^2, 42.4 °C	1.733	5.204E−11	6.548E−05	1	2.58	1.109	139	2.7701E−02	1.6967E−02
632 W/m^2, 44.9 °C	1.379	9.340E−11	5.748E−05	1	2.53	1.212	173	2.1544E−02	1.4332E−02
445 W/m^2, 46.6 °C	0.978	1.360E−10	2.048E−05	1	2.27	1.381	216	1.3947E−02	9.4445E−03

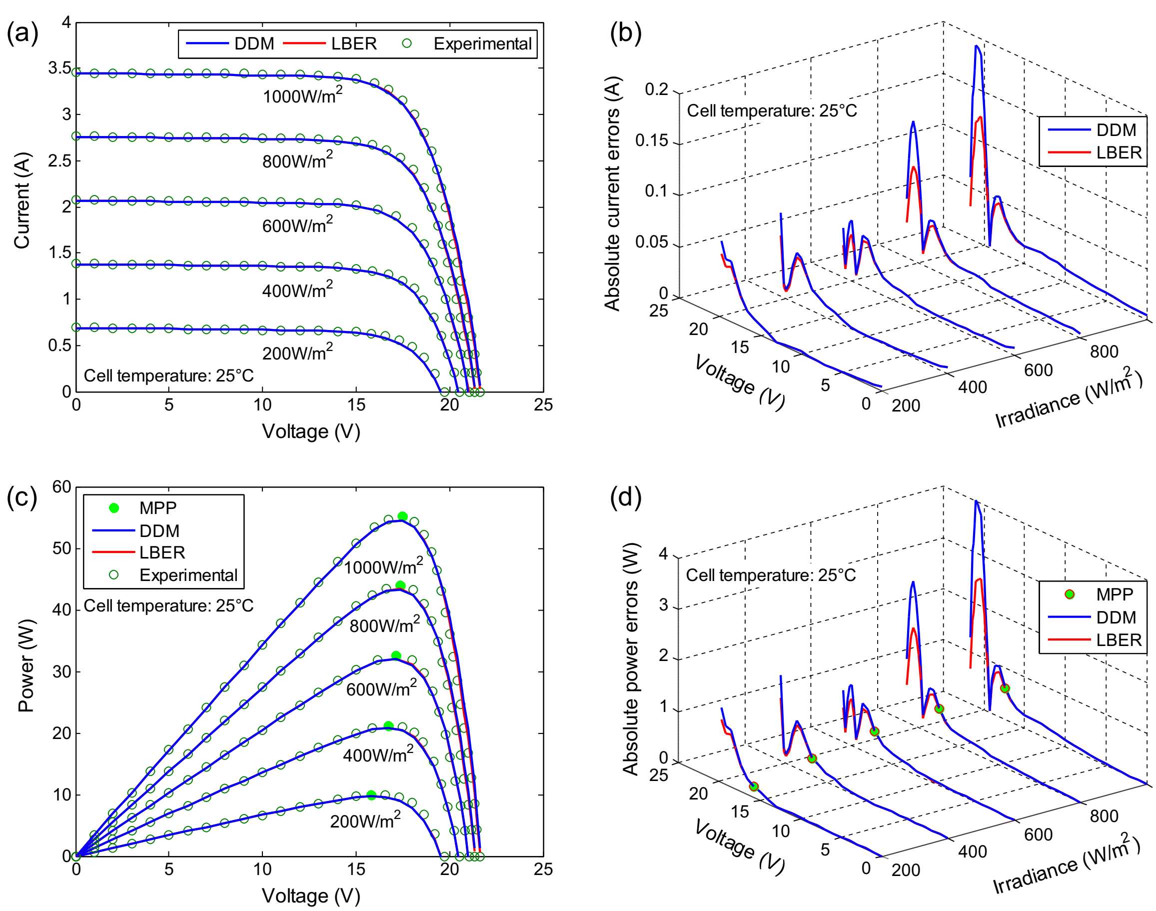

Fig. 3. Calculated curves of DDM and LBER using the experimental I–V data of SM55 module [44] at varying irradiance and the parameter values extracted by FPA [56]: (a) I–V characteristics, (b) absolute current errors, (c) P–V characteristics and (d) absolute power errors.

values are considerably smaller than those of $RMSE_{cal\_DDM}$. This confirms that under the same parameter values of I_{ph}, I_{01}, I_{02}, n_1, n_2, R_s and R_{sh}, the proposed LBER has better fitness to the experimental I–V data of all module types.

Figs. 3–8 depict the calculated I–V characteristics, P–V characteristics, and the corresponding absolute errors of DDM and LBER to compare with the experimental data of the four solar modules at varying irradiance and temperature. It can be observed from Figs. 3–8(a) and (c) that for each irradiance and cell temperature, the calculated I–V and P–V characteristics of LBER are in closer agreement to experimental data, particularly in high-voltage range. This demonstrates the proposed LBER is more accurate than

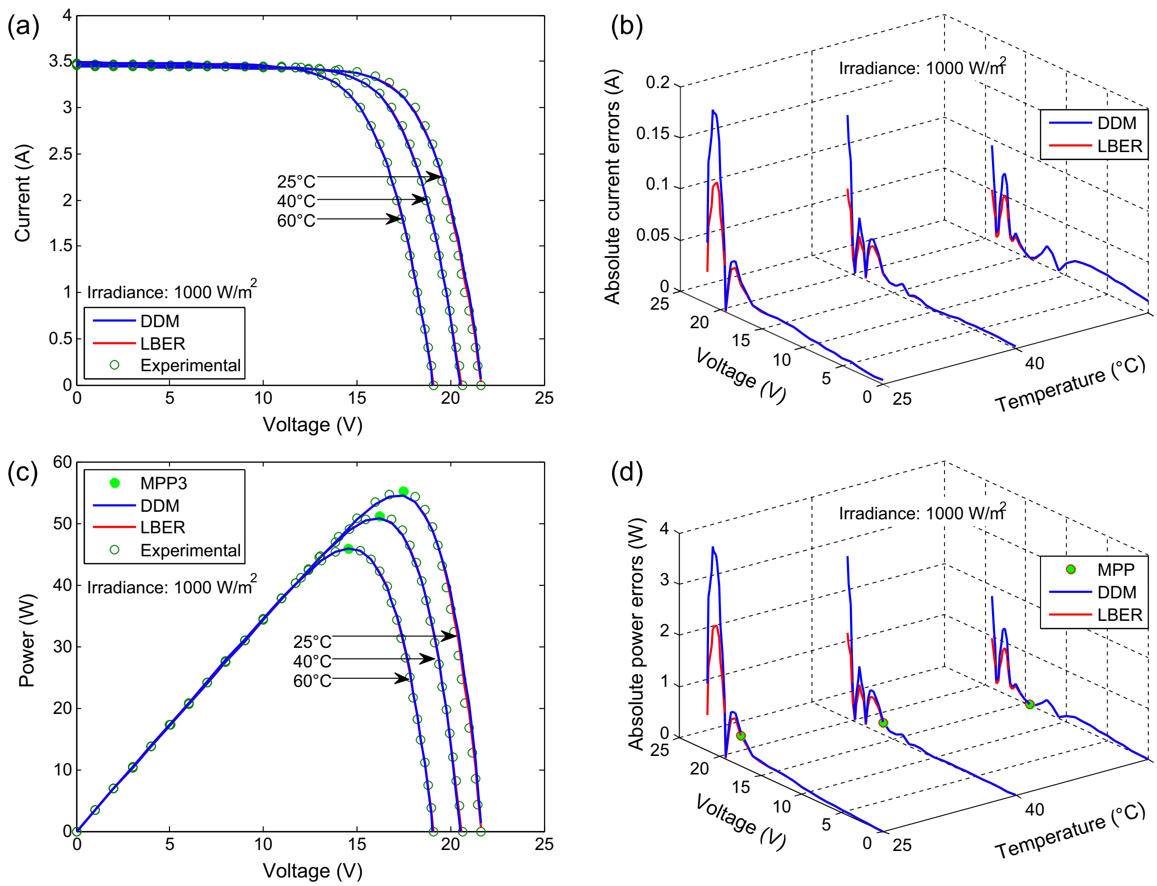

Fig. 4. Calculated curves of DDM and LBER using the experimental *I–V* data of SM55 module [44] at varying temperature and the parameter values extracted by FPA [56]: (a) *I–V* characteristics, (b) absolute current errors, (c) *P–V* characteristics and (d) absolute power errors.

DDM in representing the *I–V* and *P–V* characteristics all module types over a wide range of irradiance and temperature variations. From Figs. 3–8(b) and (d), one can observe the similarity of the absolute errors at varying irradiance and temperature. These figures indicate that the absolute errors of all module types tend to increase with the increase of irradiance and decrease as temperature rising. The only exception is the absolute errors of ST40 module increase with the increase of temperature, which can be attributed to the lower accuracy of the parameter values.

Furthermore, a close inspection of Figs. 3–8(c) and (d) reveals that the proposed LBER exhibits smaller absolute power errors around MPP compared with DDM. This means the proposed LBER can provide a closer representation to actual MPP of all module types at any irradiance and temperature conditions. The difference between the absolute power errors around MPP of DDM and LBER depends upon the accuracy of the parameter values listed in Tables 2–5. Overall, the more accurate the parameter values, the less the difference. Once the real values of the model parameters are obtained, this difference is equal to zero. It should be stressed that due to using the experimental *I–V* data, no information is available about the real values of the model parameters [48,53]. Therefore under the same parameter values, any reduction of absolute power errors is significant. Because it results in more veracious energy yield calculations in PV simulation, and hence ensures more accurate predicting of MPP of solar module/array. Consequently, the proposed LBER would be beneficial for the maximum energy harvesting of PV systems.

In summary, the results above clearly demonstrate that, comparing with DDM the proposed LBER can always present better fitness in representing the *I–V* and *P–V* characteristics of solar cells. This superiority depends not upon cell technology, irradiance and temperature, and can be further applied to forecast more accurate MPP for solar array, and hence optimize the performance and increase the efficiency of PV systems.

4. rbcNM algorithm for parameter extraction of LBER and DDM

To further investigate the performance difference between DDM and LBER, our restart-based bound constrained Nelder-Mead (rbcNM) algorithm [31] is revised in this section for parameter extraction of them. The main objective of parameter extraction of DDM and LBER is to find a set of parameter values for minimizing the errors between the calculated current and experimental current, this can be formulated using an objective function.

4.1. Objective function

Similar to Refs. [48–60], RMSE is chosen as the objective function and the optimization goal is set to minimize Eq. (19) with respect to the parameter vector $\boldsymbol{X} = [I_{ph}, I_{01}, I_{02}, n_1, n_2, R_s, R_{sh}]$.

$$RMSE_{cal}(\boldsymbol{X}) = \underset{\boldsymbol{X}\in[LB,UB]\in R^{+}}{minimize}\sqrt{\frac{1}{N}\sum\nolimits_{i=1}^{N} f_{\mathrm{M}}(V,I,\boldsymbol{X})^2} \tag{19}$$

where LB and UB are the lower and upper bounds on parameter vector $\boldsymbol{X}$, respectively. N is the number of experimental *I–V* data. The error function $f_{\mathrm{M}}(V,I,\boldsymbol{X})$ can be expressed as Eqs. (20) and (21) for DDM and LBER, respectively.

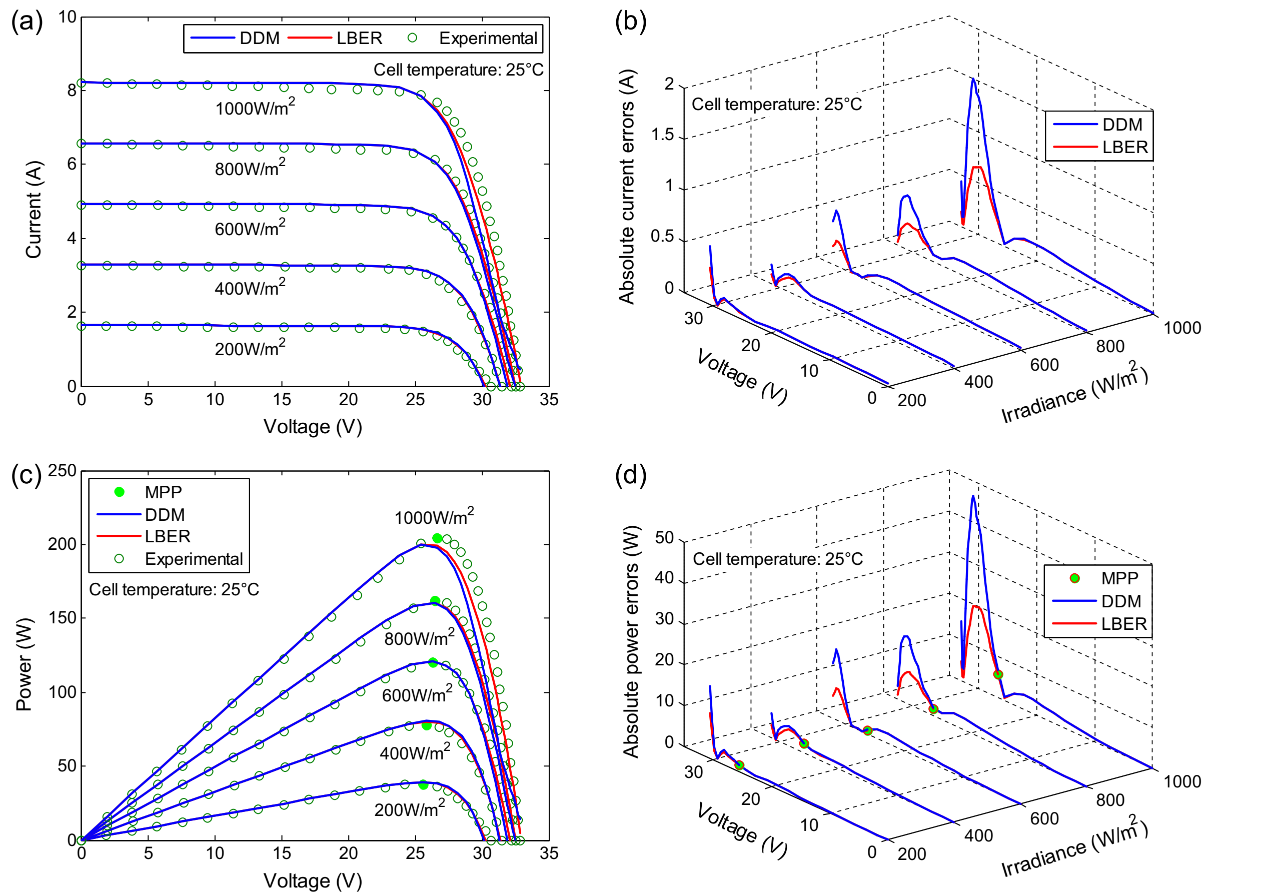

Fig. 5. Calculated curves of DDM and LBER using the experimental *I–V* data of KC200GT module [45] at varying irradiance and the parameter values extracted by FPA [56]: (a) *I–V* characteristics, (b) absolute current errors, (c) *P–V* characteristics and (d) absolute power errors.

$$f_{\mathrm{DDM}}(V,I,\boldsymbol{X}) = I_{ph} - I_{01}\left[\exp\left(\frac{V+IR_s}{n_1V_{th}}\right)-1\right] - I_{02}\left[\exp\left(\frac{V+IR_s}{n_2V_{th}}\right)-1\right] - \frac{V+IR_s}{R_{sh}} - I \tag{20}$$

$$f_{\mathrm{LBER}}(V,I,\boldsymbol{X}) = \frac{R_{sh}(I_{ph}+I_{01}+I_{02})-V}{R_s+R_{sh}} - r\frac{n_1V_{th}}{R_s}W_0(\theta_1) - (1-r)\frac{n_2V_{th}}{R_s}W_0(\theta_2) - I \tag{21}$$

It is obvious that the smaller the RMSE_{cal} value, the more accurate the parameter solution obtained. It should be noted that the parameter vector $\boldsymbol{X} = [I_{ph}, I_{01}, I_{02}, n_1, n_2, R_s, R_{sh}]$ in Eqs. (19)–(21) is treated as the unknown to be extracted from the experimental *I–V* data, whereas I_{ph}, I_{01}, I_{02}, n_1, n_2, R_s, and R_{sh} are known in Eqs. (13) and (14).

4.2. rbcNM algorithm

The Nelder-Mead (NM) algorithm is one of the most widely used direct-search method for multidimensional unconstrained optimization without derivatives [65]. NM minimizes a given objective function of m parameters by comparing one or two function evaluations at the $m + 1$ vertices of an initial simplex, and then updates the worst vertex by moving it around the centroid until it encounters a (local, at least) minimum [66]. The key attractive features of NM are simple to understand, easy to program and implement, robust, and computationally compact compared with other methods, especially those require at least m function evaluations per iteration. Given these advantages, NM has successfully been applied to many real world optimization problems in recent years. In the 1990s, NM became a standard member of Matlab libraries, where it is now called fminsearch. In 2005, John D'Errico [67] embedded lower and upper bounds into NM for solving bound constrained optimization, i.e. bound constrained Nelder-Mead (bcNM) algorithm. Although bcNM is called fminsearchbnd in Matlab, the optimization engine is still the NM itself. Therefore, fminsearchbnd is an appropriate optimizer for extracting the optimal parameter values of DDM and LBER.

Just like NM, bcNM is not very sensitive to initial values. So the parameter vector $\boldsymbol{X}$ in Eq. (19) can be initialized randomly within the searching range of [LB, UB]. For instance, for the mth parameter $\boldsymbol{X}(m)$ can be initialized as follows

$$\boldsymbol{X}_0(m) = \mathrm{LB}(m) + rand(0,1)[\mathrm{UB}(m) - \mathrm{LB}(m)] \tag{22}$$

where LB(m) and UB(m) are respectively the lower and upper bound of $\boldsymbol{X}_0(m)$, $m = 1, 2, \ldots, 7$. $rand(0,1)$ is a uniformly distributed random real number between 0 and 1.

Since the difference between the values of I_{ph} and $I_{01,2}$ is usually larger than six orders of magnitude [24] and the RMSE_{cal} values are generally over 10^{-4} (see Tables 1–5 above), here we specify TolX = 10^{-6} for the termination tolerance on parameter vector $\boldsymbol{X}$ and TolFun = 10^{-4} for the termination tolerance on objective function value. The other two termination criteria, obtained by trial and error, are as follows: the maximum number of iterations MaxIter = 5000 and the maximum number of function evaluations MaxFunEvals = 10,000.

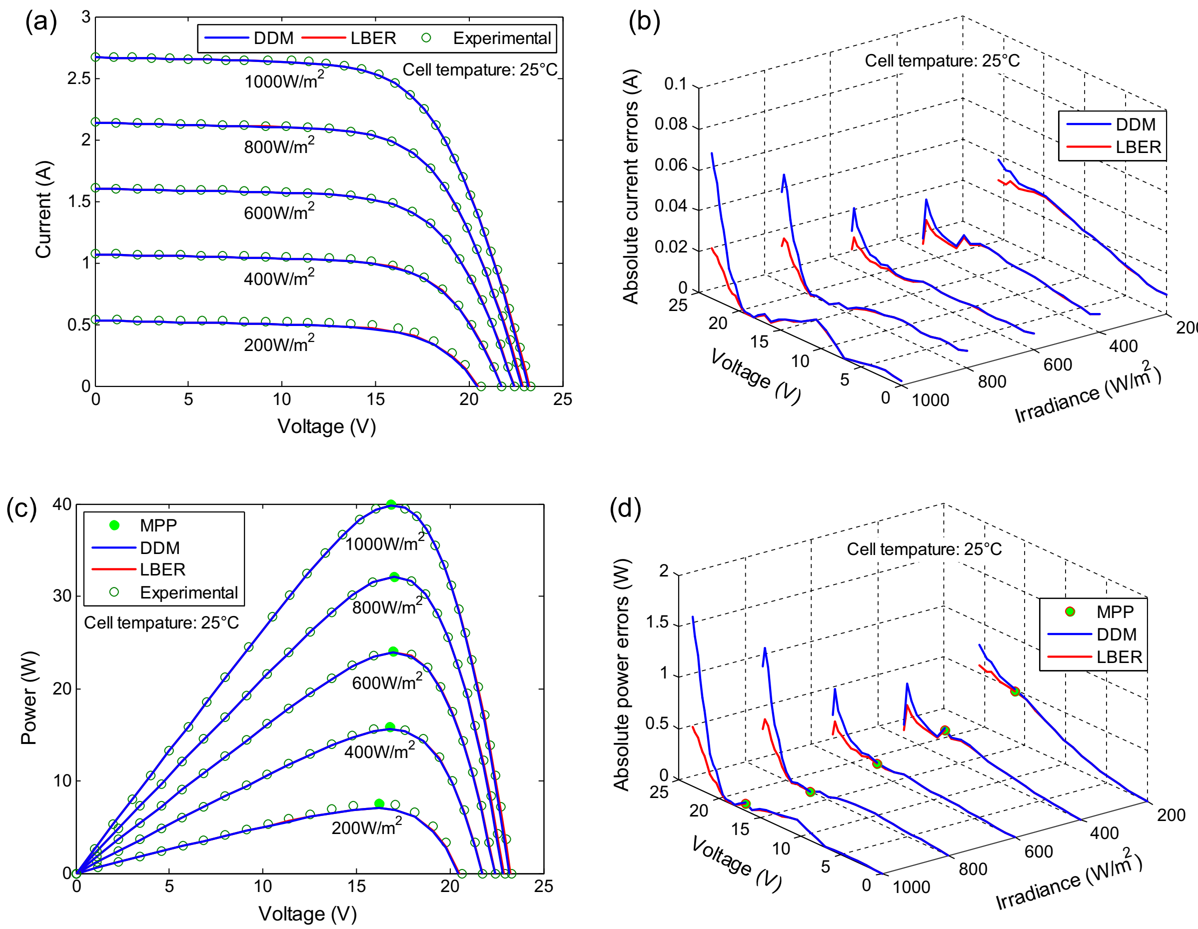

Fig. 6. Calculated curves of DDM and LBER using the experimental *I–V* data of ST40 module [46] at varying irradiance and the parameter values extracted by FPA [56]: (a) *I–V* characteristics, (b) absolute current errors, (c) *P–V* characteristics and (d) absolute power errors.

Due to the objective function values are very flat near the minimum, NM can take a large number of reflections [68] with negligible improvement in objective function value. This usually results in premature termination of iterations. In this situation, it is frequently a good idea to restart bcNM to achieve better convergence and thus improve the quality of solution. To this end, here we use the $RMSE_{cal}$ difference between before and after running bcNM, i.e. TolFun_runs $<10^{-9}$ (see Fig. 9) to decide whether to restart bcNM or not. For each restart, bcNM uses the parameter values extracted from previous run as the new initial values to further optimize objective function. After several restarts, if bcNM converges to the same objective function value, there is a good chance that this value is the optimal solution.

Fig. 9 depicts the flowchart of rbcNM algorithm for parameter extraction of LBER, where plotFcns is a plot function for plotting the convergence process, ObjFun denotes the objective function, and fval is the objective function value obtained by the *S*th run of bcNM. The flowchart for parameter extraction of DDM is similar to Fig. 9 except replacing Eqs. (18) and (21) with Eqs. (17) and (20), respectively.

5. Parameter extraction comparison between LBER and DDM

This section elaborates and compares the parameter extraction results of DDM and LBER. Two different algorithms are used to this end. One is above-mentioned rbcNM algorithm which is used for the parameter extraction of DDM and LBER of R.T.C. Franc solar cell, and the other is the reported R_{cr}-IJADE algorithm [48] which is applied to extract the optimal parameter values of DDM and LBER of foregoing four solar modules. All comparative experiments were carried on a personal laptop with an Intel Core i5-4300M processor @ 2.60 GHz, 4 GB RAM, under the Windows 7 64-bit OS.

5.1. Results for solar cell using rbcNM algorithm

To make a fair comparison between the parameter extraction performance of DDM and LBER, rbcNM algorithm is implemented under the same simulation conditions, i.e. the searching range, initial values, and termination criteria are maintained for both of them. To make the comparison more comprehensive, the searching ranges of I_{ph}, I_{01}, I_{02}, n_1, n_2, R_s and R_{sh} for R.T.C. France solar cell [43] are set the same as Refs. [48–60] and given in Table 6. Convergence speed, robustness and accuracy are used as the performance criteria to evaluate the parameter extraction results of DDM and LBER of R.T.C. France solar cell.

5.1.1. Convergence speed

Under the same simulation conditions, the convergence process of rbcNM algorithm for parameter extraction of DDM and LBER of R.T.C. France solar cell are illustrated respectively in Fig. 10(a) and (b), indicating the different $RMSE_{cal}$ values during the iterations. It is evident from Fig. 10 that the restarting strategy can effectively make bcNM to escape from local minima and thus improve the quality of the solution. From the upper left of Fig. 10(a) and (b), it can be seen that the starting $RMSE_{cal}$ value

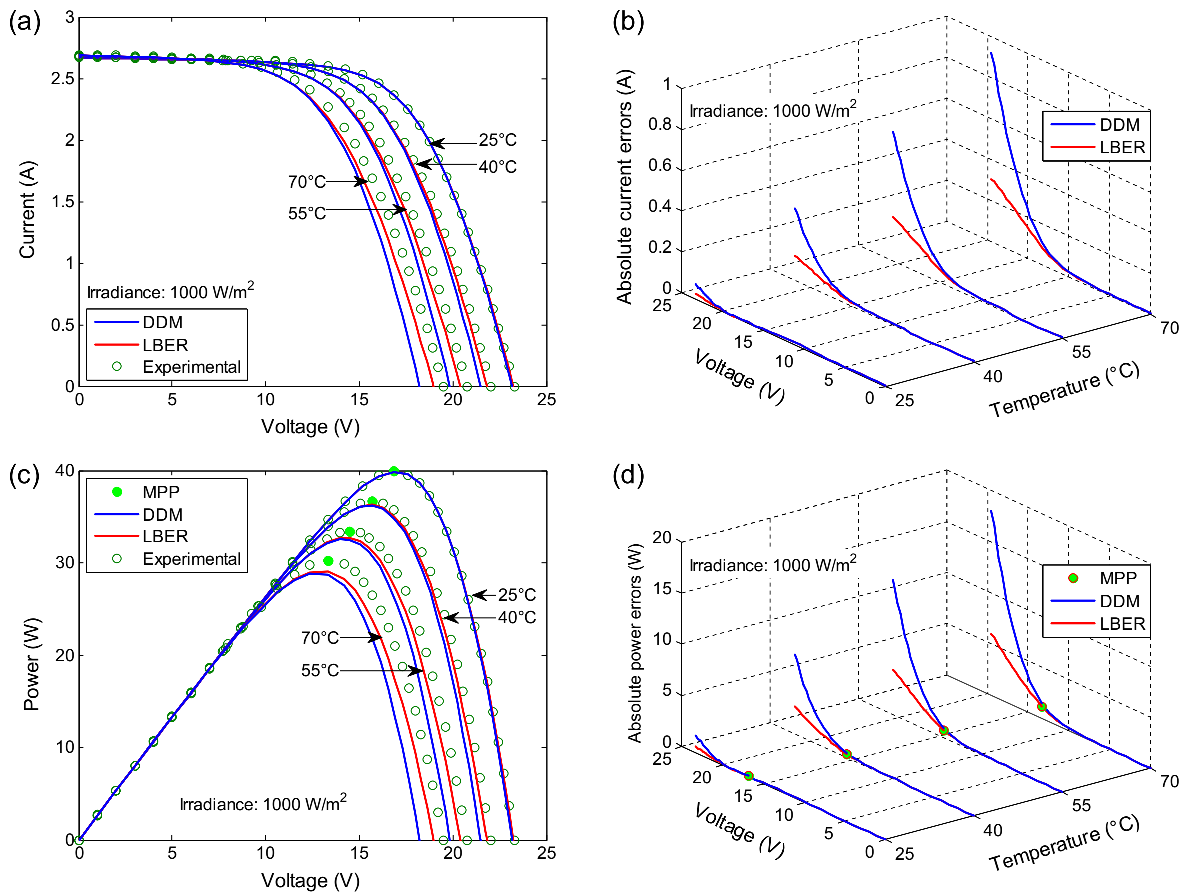

Fig. 7. Calculated curves of DDM and LBER using the experimental *I–V* data of ST40 module [46] at varying temperature and the parameter values extracted by FPA [56]: (a) *I–V* characteristics, (b) absolute current errors, (c) *P–V* characteristics and (d) absolute power errors.

of LBER (0.096991848) is much less than that of DDM (0.18141361). From the zoomed views near the minimum, the straight red[1] lines generated by the last run of bcNM indicate the rbcNM algorithm converges successfully to stable solution. It is clear that the minimum $RMSE_{cal}$ value of LBER (0.00074259259) is smaller than that of DDM (0.00098248485). But on the contrary, the total iteration number of DDM is only 3771 and much less than that of LBER (5975). This shows the convergence speed of LBER is slower than that of DDM. In addition, due to the computational time of Lambert *W*-function is 2.8–4.1 times that of exponential function [11], the convergence process of LBER is time consuming and more than 10 times slower than that of DDM.

5.1.2. Robustness

Since the parameter vector $\boldsymbol{X} = [I_{ph}, I_{01}, I_{02}, n_1, n_2, R_s, R_{sh}]$ can be initialized randomly, 50 independent runs of rbcNM algorithm are carried out for parameter extraction of DDM and LBER. The distributions of starting $RMSE_{cal}$ value and minimum $RMSE_{cal}$ value for each independent run are depicted in Fig. 11(a) and (b), respectively.

It is obvious from Fig. 11(a) that DDM and LBER have vastly different starting $RMSE_{cal}$ values under the same initial conditions, which further confirms the fitness difference discussed in Section 3. As can be seen from Fig. 11(b), the minimum $RMSE_{cal}$ values of DDM show a distinct variation. By contrast, the minimum $RMSE_{cal}$ values of LBER are very stable without any fluctuations. This confirms that the parameter values extracted from LBER are more robust than those from DDM. Furthermore, it can be seen from the top of Fig. 11(b) that the minimum $RMSE_{cal}$ values of DDM generally fall into two groups: 0.00098248 and 0.00098602, repeating 33 and 17 times respectively. From numerical point of view, the latter equals to the optimal $RMSE_{cal}$ value of SDM Eq. (2), as evidenced by the reported values from Refs. [48,49,54]. Also, we found that most of the parameter values extracted from DDM corresponding to 0.00098602 meet the conditions simultaneously: $n_1 \approx n_2 \approx n$ and $I_{01} + I_{02} = I_0$. These reveal that DDM Eq. (1) is more likely to degenerate than LBER Eq. (12). This is another proof that LBER is more robust than DDM.

5.1.3. Accuracy

It can also be seen from Fig. 11(b) that all the minimum $RMSE_{cal}$ values of LBER are considerably smaller than those of DDM. Yet it would be premature to conclude the parameter values extracted from LBER are more accurate than those from DDM, because there is a remarkable fitness difference between DDM and LBER. To prove this point, here we substitute the parameter values extracted form DDM into Eq. (18) to calculate the $RMSE_{cal}$ values corresponding to LBER. For convenience of comparison, these $RMSE_{cal}$ values are also plotted in Fig. 11(b) and marked with ‐▿‐. Clearly, these $RMSE_{cal}$ values are close and fluctuating but larger than the minimum $RMSE_{cal}$ values of LBER, which demonstrates the parameter values extracted from DDM lack robustness and are less accurate than those from LBER. From this point of view, the parameter

[1] For interpretation of color in Fig. 10, the reader is referred to the web version of this article.

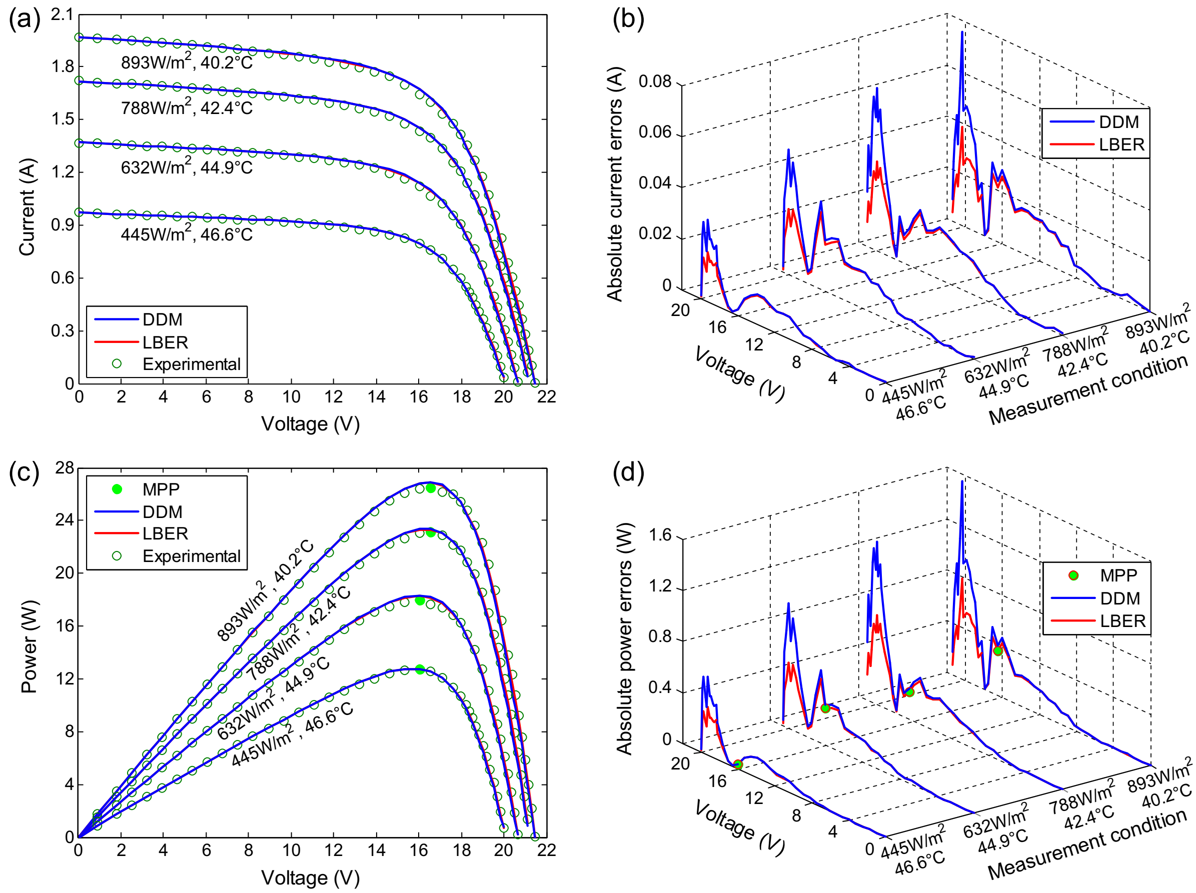

Fig. 8. Calculated curves of DDM and LBER using the experimental *I–V* data in different measurement conditions and the parameter values of an amorphous silicon triple junction module with 11 cells connected in series [47]: (a) *I–V* characteristics, (b) absolute current errors, (c) *P–V* characteristics and (d) absolute power errors.

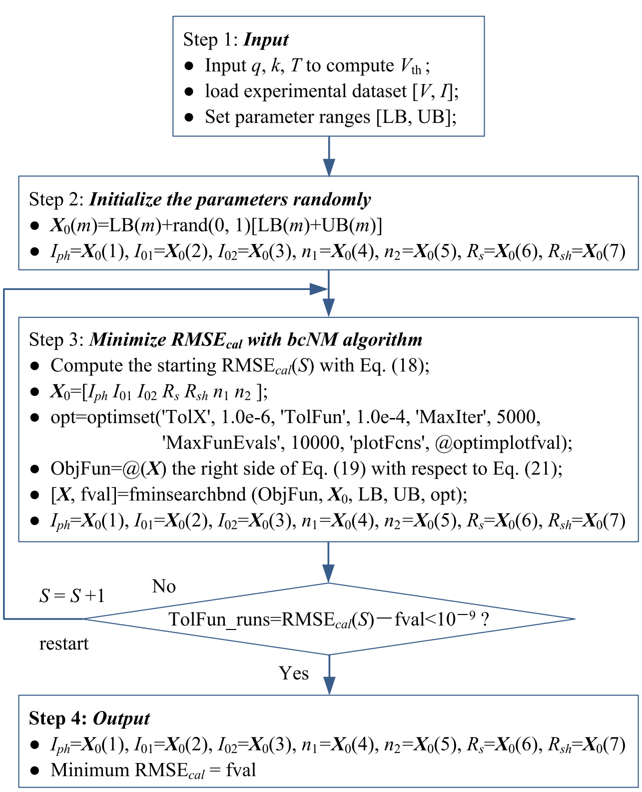

Fig. 9. Flowchart of rbcNM algorithm used for parameter extraction of the proposed LBER.

values extracted from DDM could be further optimized in LBER using rbcNM algorithm.

The optimal parameter values and minimum $RMSE_{cal}$ values extracted by rbcNM algorithm for DDM and LBER of R.T.C. France solar cell are shown in Table 6. In order to further compare the quality of the optimal parameter values extracted from DDM and LBER, they are back-substituted respectively into Eqs. (1) and (12) to reconstruct the simulated current I_{sim} at given experimental voltage point. This is simply done by utilizing fzero function or Newton method [50,52,53] when I is unknown while V is known. Note that the simulated current I_{sim} is totally different from the calculated current I_{cal} in Eqs. (13) and (14), where I and V are known. The simulated *I–V* characteristics of DDM and LBER and their respective absolute current errors for each data point are shown in Table 7 and Fig. 12.

Although Fig. 12(a) indicates the simulated *I–V* characteristics of DDM and LBER are all in excellent agreement with experimental *I–V* data, Fig. 12(b) and the last two lines of Table 7 give evidence that the sum of ACE_{sim} value and the $RMSE_{sim}$ value of LBER are smaller than those of DDM. This proves the simulated *I–V* characteristic of LBER is in higher accordance with experimental *I–V* data, and further confirms the optimal parameter values extracted from LBER are more accurate than those from DDM.

The last column of Table 7 lists all elements of r, which are computed by Eq. (5) using experimental *I–V* data and the optimal parameter values extracted from LBER. It is evident that the element of r is not fixed but increases with the increase of voltage and decreases with the increase of current. This reflects well the conduction phenomena of carriers across the junction of solar cell at different voltage and current ranges.

Table 6
Optimal parameter values and RMSE$_{cal}$ values extracted by rbcNM algorithm for DDM and LBER of R.T.C. France solar cell [43].

Model	I_{ph} (A)	I_{01} (μA)	I_{02} (μA)	n_1	n_2	R_s (Ω)	R_{sh} (Ω)	RMSE$_{cal}$
Search ranges	[0,1]	[0,1]	[0,1]	[1,2]	[1,2]	[0,0.5]	[0,100]	–
DDM	0.760781	0.225974	0.749346	1.451017	2.000000	0.036740	55.485437	9.824849E−04
LBER	0.760805	0.074265	1.000000	1.367963	1.801989	0.037726	56.219468	7.425926E−04

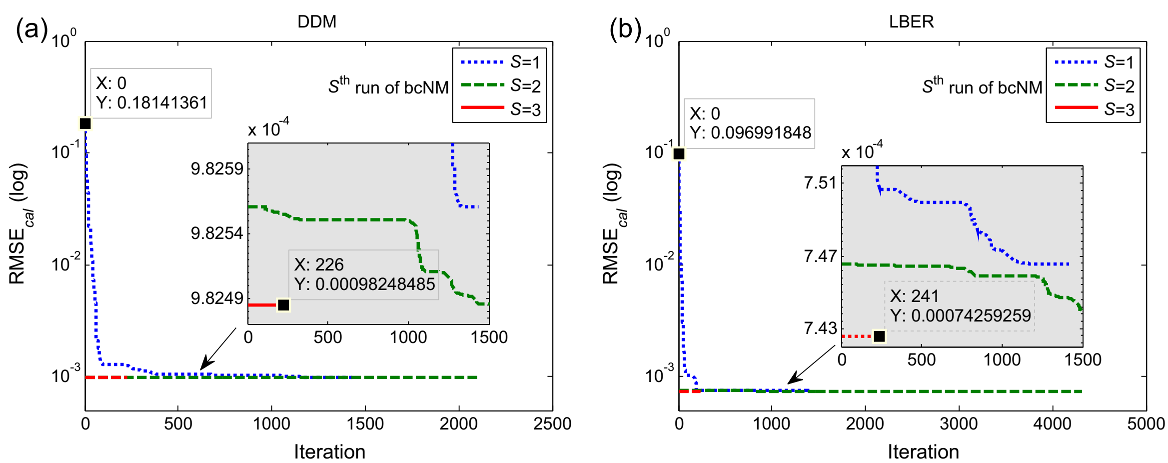

Fig. 10. Convergence curves of rbcNM algorithm during the parameter extraction process of (a) DMM and (b) LBER of R.T.C. France solar cell [43]. Insets: Magnification around the minimum RMSE$_{cal}$ values.

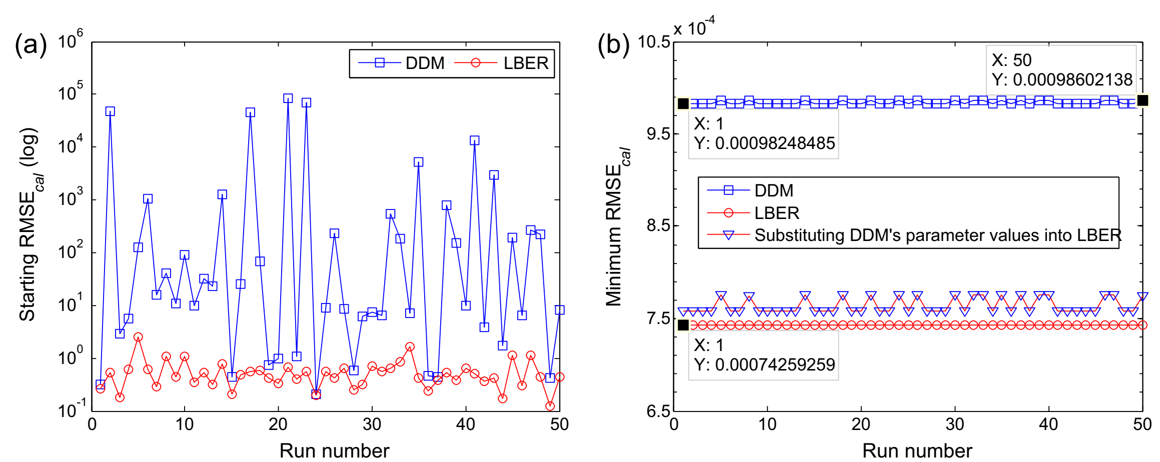

Fig. 11. Distribution of (a) starting RMSE$_{cal}$ value and (b) minimum RMSE$_{cal}$ value over 50 independent runs of rbcNM algorithm for parameter extraction of DDM and LBER of R.T.C. France solar cell [43]. For comparison, the RMSE$_{cal}$ values calculated by substituting the parameter values extracted from DDM into LBER are also plotted in (b) and marked with —▽—.

5.2. Results for solar modules using R$_{cr}$-IJADE algorithm

Given the C++ code presented in Refs. [69,70] can largely speed up the computation of Lambert *W*-function and thus improve the computational efficiency of LBER, this subsection employs the reported R$_{cr}$-IJADE algorithm [48] to extract the optimal parameter values of DDM and LBER of SM55 [44], KC200GT [45], ST40 [46] and amorphous silicon triple junction [47] modules. To be fair, the default population size $\mu = 50$ and termination criterion Max_NFEs = 20,000 of R$_{cr}$-IJADE algorithm are kept the same in parameter extraction of DDM and LBER.

Since the ranges of model parameters influence the accuracy of both the convergence speed and the results, an appropriate search range has to be specified before invoking the R$_{cr}$-IJADE algorithm. Considering the well extracted parameter values listed in Tables 2–5 and similar to Refs. [36,41,56], the search ranges of model parameters are set as: $n_{1,2} \in [1,\ 4]$, $R_s \in [0,\ 2]\,\Omega$, $R_{sh} \in [0, 5000]\,\Omega$, $I_{ph} \in [0, 2\max(I_{sc})]$ A and $I_{01,2} \in [I_{0\min},\ I_{0\max}]$ A. The lower and upper bounds on $I_{01,2}$ is computed from the experimental *I–V* data using the following equations [30]:

$$I_{0\min} = \min\left\{ I_{sc}(G,T)\left[\exp\left(\frac{V_{oc}(G,T)}{V_{th}(G,T)}\right) - 1\right]^{-1}\right\} \tag{23}$$

$$I_{0\max} = \max\left\{ I_{sc}(G,T)\left[\exp\left(\frac{V_{oc}(G,T)}{4V_{th}(G,T)}\right) - 1\right]^{-1}\right\} \tag{24}$$

where $I_{sc}(G,T)$ and $V_{oc}(G,T)$ are the short-circuit current and open-circuit voltage of certain solar module at different levels of irradiance *G* and temperature *T*, respectively.

Table 7
Simulated current data and absolute current errors of DDM and LBER reconstructed by using the experimental voltage of R.T.C. France solar cell [43] and the optimal parameter values extracted by rbcNM algorithm. For convenience, the elements of r associated with the optimal parameter values of LBER and experimental I–V data are also listed here.

Item	Experimental data		DDM		LBER		
	V (V)	I (A)	I_{sim_DDM} (A)	ACE_{sim_DDM} (A)	I_{sim_LBER} (A)	ACE_{sim_LBER} (A)	r
1	−0.2057	0.7640	0.76398342	0.00001658	0.76395257	0.00004743	0.07023633
2	−0.1291	0.7620	0.76260370	0.00060370	0.76259087	0.00059087	0.07344046
3	−0.0588	0.7605	0.76133714	0.00083714	0.76134081	0.00084081	0.08219846
4	0.0057	0.7605	0.76017400	0.00032600	0.76019261	0.00030739	0.10029555
5	0.0646	0.7600	0.75910827	0.00089173	0.75913979	0.00086021	0.12959299
6	0.1185	0.7590	0.75812202	0.00087798	0.75816335	0.00083665	0.16953507
7	0.1678	0.7570	0.75718848	0.00018848	0.75723416	0.00023416	0.21792979
8	0.2132	0.7570	0.75624423	0.00075577	0.75628483	0.00071517	0.27256162
9	0.2545	0.7555	0.75517766	0.00032234	0.75519902	0.00030098	0.32978159
10	0.2924	0.7540	0.75372286	0.00027714	0.75370754	0.00029246	0.38751209
11	0.3269	0.7505	0.75139611	0.00089611	0.75132976	0.00082976	0.44301568
12	0.3585	0.7465	0.74729616	0.00079616	0.74717728	0.00067728	0.49517833
13	0.3873	0.7385	0.73999138	0.00149138	0.73984290	0.00134290	0.54259340
14	0.4137	0.7280	0.72726488	0.00073512	0.72713722	0.00086278	0.58522809
15	0.4373	0.7065	0.70683581	0.00033581	0.70679030	0.00029030	0.62159678
16	0.4590	0.6755	0.67523011	0.00026989	0.67530974	0.00019026	0.65324445
17	0.4784	0.6320	0.63088763	0.00111237	0.63108025	0.00091975	0.67957997
18	0.4960	0.5730	0.57214027	0.00085973	0.57237885	0.00062115	0.70149805
19	0.5119	0.4990	0.49957059	0.00057059	0.49976153	0.00076153	0.71948758
20	0.5265	0.4130	0.41355632	0.00055632	0.41362248	0.00062248	0.73452530
21	0.5398	0.3165	0.31724207	0.00074207	0.31715731	0.00065731	0.74690434
22	0.5521	0.2120	0.21208148	0.00008148	0.21187756	0.00012244	0.75730246
23	0.5633	0.1035	0.10267156	0.00082844	0.10243118	0.00106882	0.76591302
24	0.5736	−0.0100	−0.00929723	0.00070277	−0.00946344	0.00053656	0.77303698
25	0.5833	−0.1230	−0.12439038	0.00139038	−0.12435547	0.00135547	0.77934018
26	0.5900	−0.2100	−0.20914692	0.00085308	−0.20888277	0.00111723	0.78323784
Sum of ACE_{sim}	–	–	–	0.01731854	–	0.01700214	–
$RMSE_{sim}$	–	–	–	7.575855E−04	–	7.419475E−04	–

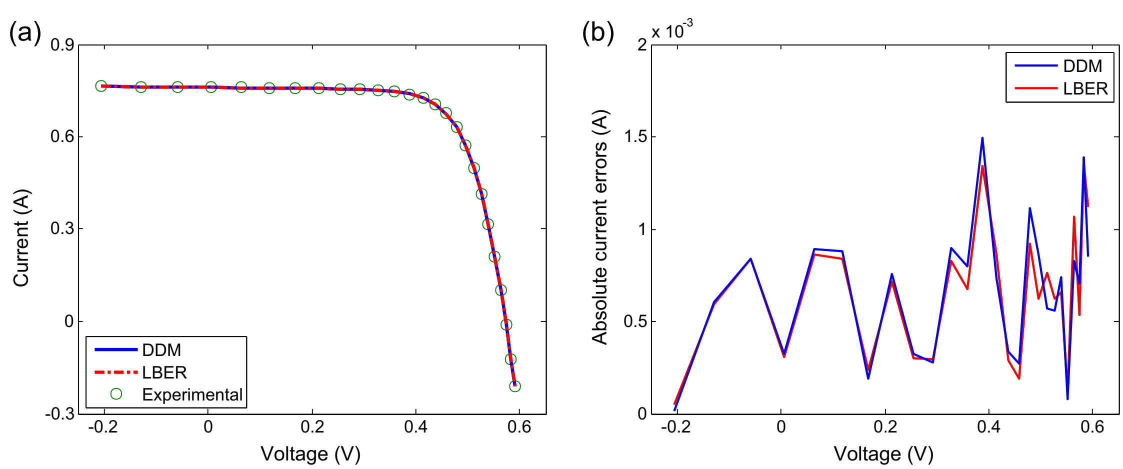

Fig. 12. Simulated curves of DDM and LBER reconstructed using the experimental voltage data of R.T.C. France solar cell [43] and the optimal parameter values extracted by rbcNM algorithm: (a) I–V characteristics, (b) absolute current errors.

For most solar modules, the value of n_1 is within the range between 1 and 2, while the value of n_2 can vary up to 4 [36,41,56]. Since Eq. (23) implies $n_1 = 1$ and Eq. (24) implies $n_2 = 4$, the value of I_{01} and I_{02} will be greater than $I_{0\min}$ and less than $I_{0\max}$. Therefore, the assignment of $I_{01,2} \in [I_{0\min}, I_{0\max}]$ is reasonable and valid. Moreover, since $I_{0\min}$ and $I_{0\max}$ are computed from the experimental I–V data rather than nominal datasheet information, this assignment can be applied to any type of solar cell/module even at different stages of performance degradation.

Under the same simulation conditions, 50 independent runs of R_{cr}-IJADE algorithm are executed in Visual Studio 2013 for parameter extraction of DDM and LBER of the four modules. The optimal parameter values and minimum $RMSE_{cal}$ values extracted from DDM and LBER are summarized in Table 8–11, respectively. To verify the accuracy of the optimal parameter values, just like before they are returned to Eqs. (1) and (12) respectively and fzero function is used to reconstruct the simulated I–V characteristics and the corresponding absolute errors of DDM and LBER. The obtained results along with the experimental I–V data of the four solar modules are plotted in Figs. 13–16 respectively to observe the agreement among them. For convenience, the obtained $RMSE_{sim}$ values are listed in the last column of Tables 8–11.

In a similar manner to the previous case, it can be seen from Figs. 13–16(a) and (c) that both the simulated I–V characteristics of DDM and LBER coincide well with the experimental I–V data, to the extent that they could not be distinguished from each other. Nevertheless, Figs. 13–16(b) and (d) give evidence that most of the absolute current errors of LBER are lower than those of DDM,

Table 8
Optimal parameter values and $RMSE_{cal}$ values extracted by R_{cr}-IJADE algorithm [48] for DDM and LBER of SM55 module [44] at different irradiance and temperature. For convenience, the reconstructed $RMSE_{sim}$ values are also listed here.

Irrad. and temp.	Model	I_{ph} (A)	I_{01} (A)	I_{02} (A)	n_1	n_2	R_s (Ω)	R_{sh} (Ω)	$RMSE_{cal}$	$RMSE_{sim}$
200 W/m², 25 °C	DDM	0.6944	1.2537E−09	4.8517E−09	1.1391	1.1574	0.5445	366.6775	2.1995E−03	2.0216E−03
	LBER	0.6944	6.1122E−09	5.4901E−10	1.1532	3.3890	0.5424	366.7849	2.0214E−03	2.0214E−03
400 W/m², 25 °C	DDM	1.3882	3.4151E−10	5.0629E−10	1.0061	1.4986	0.7258	345.7318	9.3486E−03	6.0978E−03
	LBER	1.3881	3.5703E−10	3.0879E−09	1.0093	1.3590	0.7036	346.8849	6.0354E−03	6.0337E−03
600 W/m², 25 °C	DDM	2.0799	2.6544E−10	2.7580E−10	1.0002	1.2180	0.6344	361.8583	1.2722E−02	8.5062E−03
	LBER	2.0798	2.6704E−10	3.0130E−10	1.0002	1.2340	0.6262	355.6894	8.3457E−03	8.3451E−03
800 W/m², 25 °C	DDM	2.7687	4.7332E−10	2.5047E−10	1.0280	1.2359	0.5412	398.9244	1.5000E−02	1.0817E−02
	LBER	2.7704	6.5711E−10	2.6384E−10	1.0425	3.3019	0.5277	360.0239	1.0686E−02	1.0686E−02
1000 W/m², 25 °C	DDM	3.4589	3.3008E−10	1.2343E−09	1.0152	1.3790	0.5172	435.5784	2.2918E−02	1.5275E−02
	LBER	3.4647	2.8538E−10	7.8606E−08	1.0091	1.7128	0.5073	334.0537	1.4504E−02	1.4494E−02
1000 W/m², 40 °C	DDM	3.4709	8.5126E−09	1.7289E−07	1.0762	1.5082	0.4984	330.0379	1.6886E−02	1.1125E−02
	LBER	3.4704	4.7795E−09	9.0822E−07	1.0475	1.6524	0.4995	352.5948	1.0833E−02	1.0809E−02
1000 W/m², 60 °C	DDM	3.4780	7.2722E−08	1.0075E−06	1.0633	1.3600	0.4879	400.3159	1.4127E−02	1.0289E−02
	LBER	3.4754	4.9901E−08	6.8537E−06	1.0360	1.6252	0.4923	522.3561	1.0183E−02	1.0160E−02

Table 9
Optimal parameter values and $RMSE_{cal}$ values extracted by R_{cr}-IJADE algorithm [48] for DDM and LBER of KC200GT module [45] at different irradiance and 25 °C. For convenience, the reconstructed $RMSE_{sim}$ values are also listed here.

Irradiance	Model	I_{ph} (A)	I_{01} (A)	I_{02} (A)	n_1	n_2	R_s (Ω)	R_{sh} (Ω)	$RMSE_{cal}$	$RMSE_{sim}$
200 W/m²	DDM	1.6133	3.9896E−10	5.4737E−10	1.0018	1.2258	1.1168	1090.3559	1.0397E−02	8.4331E−03
	LBER	1.6159	4.6042E−10	1.1439E−09	1.0072	2.7871	1.0831	854.6592	8.0770E−03	8.0770E−03
400 W/m²	DDM	3.2714	2.5896E−09	4.0012E−10	1.0849	1.3092	0.4719	366.9248	7.6686E−03	6.9590E−03
	LBER	3.2726	1.6823E−09	4.4341E−10	1.0630	1.3629	0.4885	349.6892	6.8643E−03	6.8643E−03
600 W/m²	DDM	4.9037	1.8831E−08	4.0220E−10	1.2002	3.9946	0.3063	346.4006	3.2512E−02	2.5927E−02
	LBER	4.9139	4.9301E−10	2.0207E−09	1.0752	1.0916	0.3615	254.5031	2.3566E−02	2.3566E−02
800 W/m²	DDM	6.5585	1.1931E−09	4.0086E−10	1.0479	1.2647	0.3084	205.2078	2.6180E−02	2.1576E−02
	LBER	6.5574	7.2389E−10	4.0909E−10	1.0251	1.3073	0.3154	192.4686	1.9488E−02	1.9488E−02
1000 W/m²	DDM	8.2232	5.2177E−10	8.2307E−09	1.0142	1.3187	0.2460	128.8551	2.8066E−02	1.8927E−02
	LBER	8.2280	4.1837E−10	7.4484E−09	1.0025	1.4427	0.2534	121.1342	1.8520E−02	1.8516E−02

Table 10
Optimal parameter values and $RMSE_{cal}$ values extracted by R_{cr}-IJADE algorithm [48] for DDM and LBER of ST40 module [46] at different irradiance and temperature. For convenience, the reconstructed $RMSE_{sim}$ values are also listed here.

Irrad. and temp.	Model	I_{ph} (A)	I_{01} (A)	I_{02} (A)	n_1	n_2	R_s (Ω)	R_{sh} (Ω)	$RMSE_{cal}$	$RMSE_{sim}$
200 W/m², 25 °C	DDM	0.5400	1.3945E−06	2.9025E−08	1.4964	1.4964	1.1767	589.2470	8.0288E−04	7.5894E−04
	LBER	0.5400	7.7054E−08	1.2894E−06	1.4917	1.4917	1.1932	586.9796	7.5785E−04	7.5785E−04
400 W/m², 25 °C	DDM	1.0755	3.4420E−06	1.1240E−09	1.6000	1.6000	0.9338	436.1498	2.5578E−03	2.0295E−03
	LBER	1.0763	1.1237E−09	2.5445E−06	1.5630	1.5630	0.9951	415.2014	1.9571E−03	1.9571E−03
600 W/m², 25 °C	DDM	1.6133	8.8059E−08	1.8563E−06	1.5306	1.5306	1.0867	342.0714	1.9890E−03	1.1542E−03
	LBER	1.6137	8.2089E−07	9.0120E−07	1.5172	1.5172	1.1010	334.4062	1.1207E−03	1.1207E−03
800 W/m², 25 °C	DDM	2.1498	3.0313E−08	1.9884E−06	1.5349	1.5349	1.1114	333.7400	2.7476E−03	1.5231E−03
	LBER	2.1509	1.1243E−09	1.6512E−06	1.5132	1.5132	1.1288	318.2077	1.4151E−03	1.4151E−03
1000 W/m², 25 °C	DDM	2.6769	1.2694E−06	7.5080E−07	1.5339	1.5339	1.1215	428.8041	2.0965E−03	1.9059E−03
	LBER	2.6771	1.8427E−06	1.2015E−07	1.5308	1.5308	1.1235	423.8512	1.9034E−03	1.9034E−03
1000 W/m², 40 °C	DDM	2.6856	5.1482E−06	7.6839E−07	1.4966	1.4966	1.1445	349.2110	2.2609E−03	1.7325E−03
	LBER	2.6860	3.8389E−06	1.8306E−06	1.4918	1.4918	1.1479	343.5295	1.7256E−03	1.7256E−03
1000 W/m², 55 °C	DDM	2.6876	2.6429E−05	6.9377E−07	1.5242	1.5242	1.1280	432.3328	1.7120E−03	1.5615E−03
	LBER	2.6876	2.5817E−06	2.4582E−05	1.5244	1.5244	1.1279	432.9641	1.5615E−03	1.5615E−03
1000 W/m², 70 °C	DDM	2.7024	5.3710E−05	2.2557E−04	1.4603	2.5850	1.1552	336.6433	1.5664E−03	8.1973E−04
	LBER	2.7020	1.5261E−05	1.4838E−04	1.3420	1.8364	1.1703	345.8624	8.0435E−04	8.0102E−04

Table 11
Optimal parameter values and $RMSE_{cal}$ values extracted by R_{cr}-IJADE algorithm [48] for DDM and LBER of an amorphous silicon triple junction module with 11 cells connected in series [47]. For convenience, the reconstructed $RMSE_{sim}$ values are also listed here.

Measurement conditions	Model	I_{ph} (A)	I_{01} (A)	I_{02} (A)	n_1	n_2	R_s (Ω)	R_{sh} (Ω)	$RMSE_{cal}$	$RMSE_{sim}$
893 W/m², 40.2 °C	DDM	1.9881	3.6618E−07	5.2424E−04	1.5883	3.6763	0.6479	101.2037	6.7916E−03	5.5579E−03
	LBER	1.9846	1.4535E−07	1.0205E−03	1.4992	3.9965	0.6796	114.7715	4.9936E−03	4.9580E−03
788 W/m², 42.4 °C	DDM	1.7335	1.3671E−07	2.7081E−04	1.4855	3.1983	0.6703	115.2780	3.5614E−03	2.8225E−03
	LBER	1.7338	2.4229E−09	2.0080E−04	1.1942	2.9544	0.8139	120.2432	2.5870E−03	2.5575E−03
632 W/m², 44.9 °C	DDM	1.3775	5.0387E−08	2.0739E−04	1.3829	2.9441	0.6472	150.8265	3.5700E−03	3.1124E−03
	LBER	1.3760	6.8866E−08	5.1769E−04	1.3991	3.4348	0.6823	167.1530	2.9958E−03	2.9854E−03
445 W/m², 46.6 °C	DDM	0.9798	3.8586E−07	6.0602E−05	1.5278	2.8930	0.7017	172.1842	2.8438E−03	2.4244E−03
	LBER	0.9782	2.0143E−07	4.5077E−04	1.4597	3.9659	0.7914	195.5265	2.1194E−03	2.1121E−03

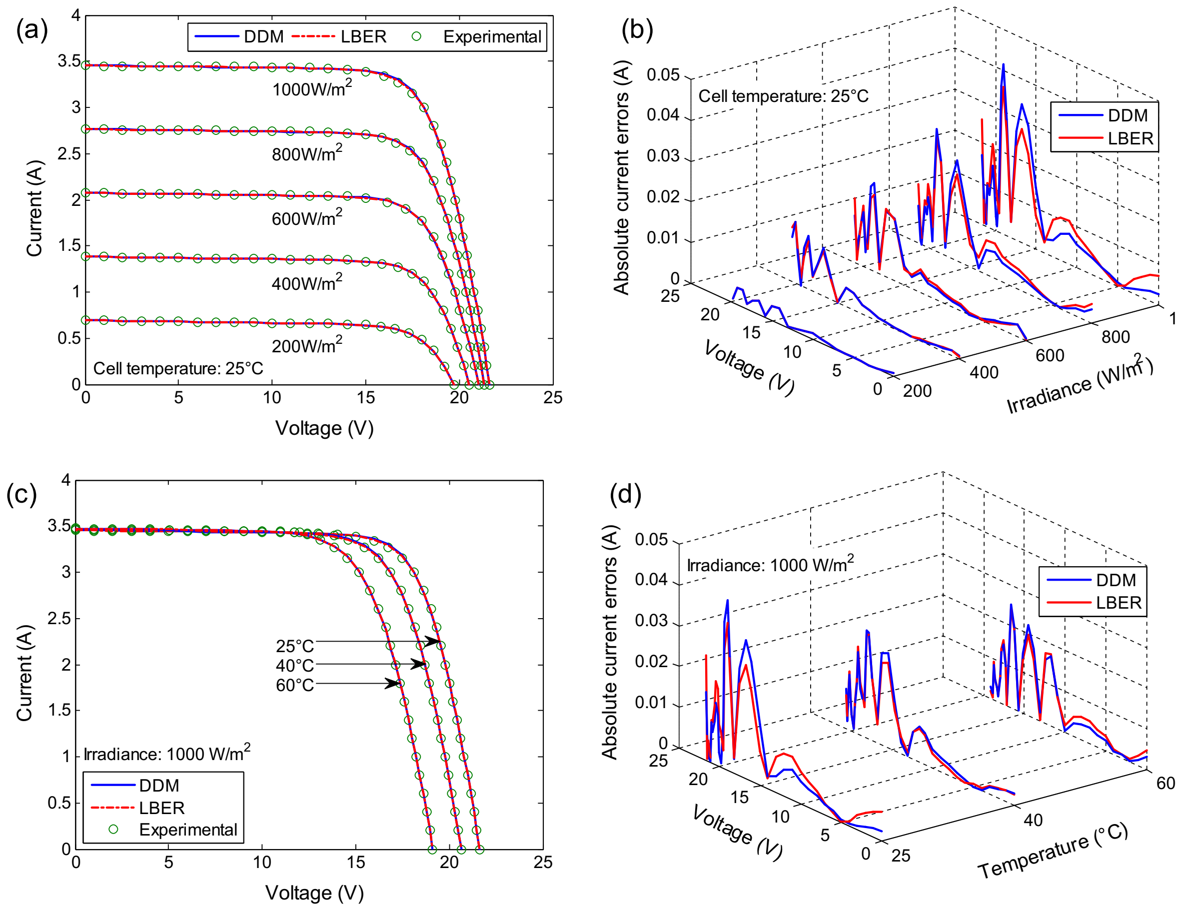

Fig. 13. Simulated curves of DDM and LBER reconstructed using the experimental voltage data of SM55 module [44] and the optimal parameter values extracted by R_{cr}-IJADE algorithm [48]: (a) and (c) *I–V* characteristics, (b) and (d) absolute current errors.

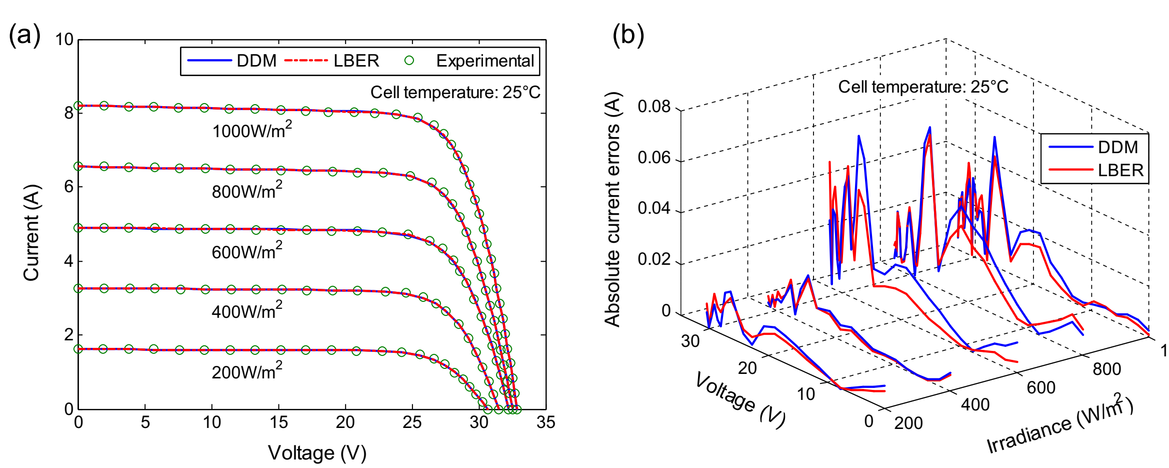

Fig. 14. Simulated curves of DDM and LBER reconstructed using the experimental voltage data of KC200GT module [45] and the optimal parameter values extracted by R_{cr}-IJADE algorithm [48]: (a) *I–V* characteristics, (b) absolute current errors.

which suggests LBER has better agreement with the experiment *I–V* data. Furthermore, it can be observed from the last two columns of Tables 8–11 that all the $RMSE_{cal}$ values and $RMSE_{sim}$ values of LBER are smaller than those of DDM. These results confirm that the optimal parameters extracted from LBER are more accurate than those from DDM. It is important to highlight here that although the $RMSE_{sim}$ values of DDM is very close to those of LBER, however, there is no information about the real values of the parameters; therefore, any reduction in $RMSE_{sim}$ value is significant, because it results in improvement in the knowledge about the real values of the parameters [48,53].

Moreover, it can be observed from Table 10 that most of the values of $n_1$equal to those of n_2. These equivalences between n_1 and n_2 meant that DDM Eq. (1) degenerates into SDM Eq. (2), and the proposed LBER Eq. (12) reduces to EESDM Eq. (3). This degeneration can be attributed to the experimental *I–V* data of ST40 module

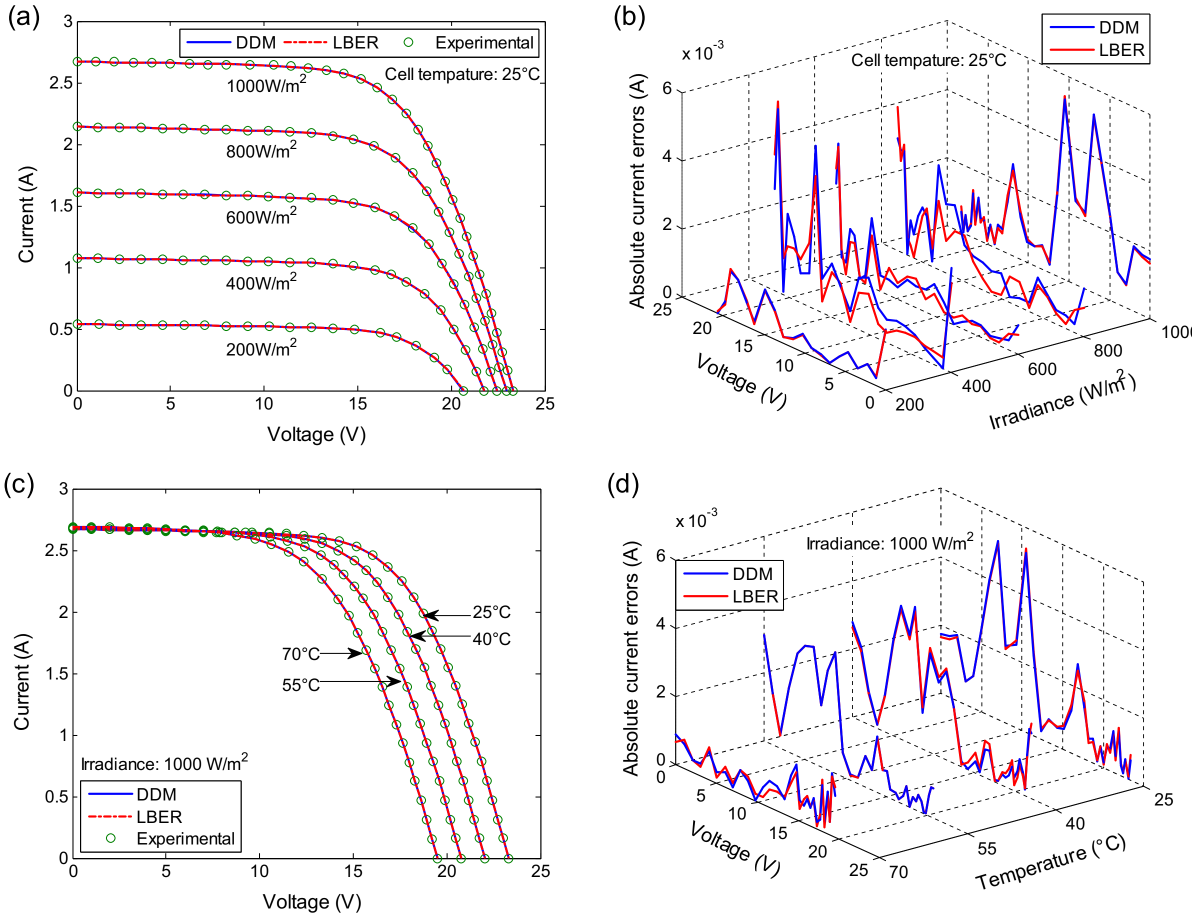

Fig. 15. Simulated curves of DDM and LBER reconstructed using the experimental voltage data of ST40 module [46] and the optimal parameter values extracted by R_{cr}-IJADE algorithm [48]: (a) and (c) *I–V* characteristics, (b) and (d) absolute current errors.

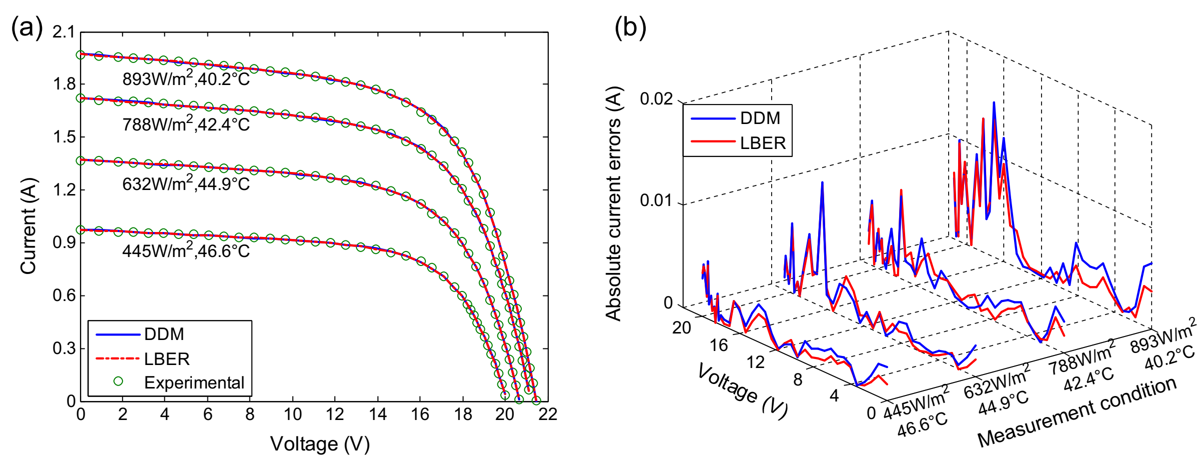

Fig. 16. Simulated curves of DDM and LBER reconstructed using the experimental voltage data of amorphous silicon triple junction module [47] and the optimal parameter values extracted by R_{cr}-IJADE algorithm [48]: (a) *I–V* characteristics, (b) absolute current errors.

are extracted from the *I–V* curves [46] generated by PVsyst, which is based on standard one-diode-model [64]. Nevertheless, it can be seen from Table 10 that the parameter values extracted from LBER are still more accurate than those from DDM, since all the $RMSE_{sim}$ values of LBER are smaller than those of DDM.

With regard to the computation speed, it is observed that the computation times of R_{cr}-IJADE algorithm for parameter extraction of LBER run about 3 times slower than those of DDM. This is certainly a big step forward compared with that without acceleration of Lambert *W*-function as stated in Section 5.1.1.

6. Conclusion

This paper presents a Lambert *W*-function based exact representation for physics-based double diode model of solar cells. The proposed LBER is closely linked with but different from

DDM. On the one hand, both of them have identical parameters and should theoretically be equivalent to each other. But on the other hand, due to the intervention of Lambert *W*-function or not, they are expressed and calculated in different ways and hence have different performance. The difference between DDM and the proposed LBER mainly lies in two aspects: (1) fitness to experimental *I*–*V* data of solar cells, and (2) parameter extraction performance. In this paper, the fitness difference between DDM and LBER is objectively validated by the reported parameter values and experimental *I*–*V* data of a solar cell and four solar modules from different technologies. The comparison results demonstrate that under the same parameter values, the proposed LBER can always present better fitness in representing the *I*–*V* and *P*–*V* characteristics of solar cells and provide a closer representation to actual MPP of solar modules. The parameter extraction difference between DDM and LBER is verified by our rbcNM algorithm and the reported R_{cr}-IJADE algorithm. The comparison results reveal that, the parameter values extracted from LBER using two algorithms are more accurate and robust than those from DDM despite more time consuming. These results put into evidence that the proposed LBER achieves better performance than DDM. As an improved version of DDM, the proposed LBER is quite promising and envisaged to be a valuable model for PV simulation.

The source codes of fitness comparison and rbcNM algorithm are available from the first author upon request.

Acknowledgments

The authors would like to thank the anonymous reviewers for their constructive suggestions. This work was supported by the Scientific Research Foundation of the Higher Education Institutions of Henan Province [Grant number 15A480006] and the National Natural Science Foundation of China [Grant numbers 51576060 and U1304528].

The authors gratefully acknowledge Dr. W. Gong and Dr. Darko Veberic for their kindly providing the source codes of R_{cr}-IJADE algorithm and C++ implementation of Lambert *W*-function.

References

[1] Wolf M, Noel GT, Stirn RJ. Investigation of the double exponential in the current–voltage characteristics of silicon solar cells. IEEE Trans Electron Devices 1977;24:419–28. http://dx.doi.org/10.1109/T-ED.1977.18750.
[2] Chin VJ, Salam Z, Ishaque K. Cell modelling and model parameters estimation techniques for photovoltaic simulator application: a review. Appl Energy 2015;154:500–19. http://dx.doi.org/10.1016/j.apenergy.2015.05.035.
[3] Humada AM, Hojabri M, Mekhilef S, Hamada HM. Solar cell parameters extraction based on single and double-diode models: a review. Renew Sustain Energy Rev 2016;56:494–509. http://dx.doi.org/10.1016/j.rser.2015.11.051.
[4] Attivissimo F, Adamo F, Carullo A, Lanzolla AML, Spertino F, Vallan A. On the performance of the double-diode model in estimating the maximum power point for different photovoltaic technologies. Measurement 2013;46:3549–59. http://dx.doi.org/10.1016/j.measurement.2013.06.032.
[5] Ishaque K, Salam Z. A review of maximum power point tracking techniques of PV system for uniform insolation and partial shading condition. Renew Sustain Energy Rev 2013;19:475–88. http://dx.doi.org/10.1016/j.rser.2012.11.032.
[6] Kharb RK, Shimi SL, Chatterji S, Ansari MF. Modeling of solar PV module and maximum power point tracking using ANFIS. Renew Sustain Energy Rev 2014;33:602–12. http://dx.doi.org/10.1016/j.rser.2014.02.014.
[7] Liu Y, Li M, Ji X, Luo X, Wang M, Zhang Y. A comparative study of the maximum power point tracking methods for PV systems. Energy Convers Manage 2014;85:809–16. http://dx.doi.org/10.1016/j.enconman.2014.01.049.
[8] Fathabadi H. Two novel techniques for increasing energy efficiency of photovoltaic-battery systems. Energy Convers Manage 2015;105:149–66. http://dx.doi.org/10.1016/j.enconman.2015.07.036.
[9] Kheldoun A, Bradai R, Boukenoui R, Mellit A. A new golden section method-based maximum power point tracking algorithm for photovoltaic systems. Energy Convers Manage 2016;111:125–36. http://dx.doi.org/10.1016/j.enconman.2015.12.039.
[10] Femia N, Petrone G, Spagnuolo G, Vitelli M. Power electronics and control techniques for maximum energy harvesting in photovoltaic systems. CRC Press; 2012.
[11] Fukushima T. Precise and fast computation of Lambert W-functions without transcendental function evaluations. J Comput Appl Math 2013;244:77–89. http://dx.doi.org/10.1016/j.cam.2012.11.021.
[12] Jain A, Kapoor A. Exact analytical solutions of the parameters of real solar cells using Lambert W-function. Sol Energy Mater Sol Cells 2004;81:269–77. http://dx.doi.org/10.1016/j.solmat.2003.11.018.
[13] Chen Y, Wang X, Li D, Hong R, Shen H. Parameters extraction from commercial solar cells I-V characteristics and shunt analysis. Appl Energy 2011;88:2239–44. http://dx.doi.org/10.1016/j.apenergy.2010.12.048.
[14] Fathabadi H. Novel neural-analytical method for determining silicon/plastic solar cells and modules characteristics. Energy Convers Manage 2013;76:253–9. http://dx.doi.org/10.1016/j.enconman.2013.07.055.
[15] Lineykin S, Averbukh M, Kuperman A. An improved approach to extract the single-diode equivalent circuit parameters of a photovoltaic cell/panel. Renew Sustain Energy Rev 2014;30:282–9. http://dx.doi.org/10.1016/j.rser.2013.10.015.
[16] Xu Y, Kong X, Zeng Y, Tao S, Xiao X. A modeling method for photovoltaic cells using explicit equations and optimization algorithm. Int J Electr Power Energy Syst 2014;59:23–8. http://dx.doi.org/10.1016/j.ijepes.2014.01.017.
[17] Batzelis EI, Routsolias IA, Papathanassiou SA. An explicit PV string model based on the Lambert W function and simplified MPP expressions for operation under partial shading. IEEE Trans Sustain Energy 2014;5:301–12. http://dx.doi.org/10.1109/TSTE.2013.2282168.
[18] Fathabadi H. Lambert W function-based technique for tracking the maximum power point of PV modules connected in various configurations. Renew Energy 2015;74:214–26. http://dx.doi.org/10.1016/j.renene.2014.07.059.
[19] Batzelis EI, Kampitsis GE, Papathanassiou SA, Manias SN. Direct MPP calculation in terms of the single-diode PV model parameters. IEEE Trans Energy Convers 2015;30:226–36. http://dx.doi.org/10.1109/TEC.2014.2356017.
[20] Ding J, Radhakrishnan R. A new method to determine the optimum load of a real solar cell using the Lambert W-function. Sol Energy Mater Sol Cells 2008;92:1566–9. http://dx.doi.org/10.1016/j.solmat.2008.07.004.
[21] Roshan YM, Moallem M. Maximum power point tracking using boost converter input resistance control by means of Lambert W-Function. In: 2012 3rd IEEE International symposium on power electronics for distributed generation systems (PEDG). p. 195–9. http://dx.doi.org/10.1109/PEDG.2012.6254000.
[22] Zhang Z, Ji Y, Cheng X, Zeng L. Universal analytical solution to the optimum load of the solar cell. Renew Energy 2015;83:55–60. http://dx.doi.org/10.1016/j.renene.2015.04.006.
[23] Ortiz-Conde A, García Sánchez FJ, Muci J. New method to extract the model parameters of solar cells from the explicit analytic solutions of their illuminated I-V characteristics. Sol Energy Mater Sol Cells 2006;90:352–61. http://dx.doi.org/10.1016/j.solmat.2005.04.023.
[24] Zhang C, Zhang J, Hao Y, Lin Z, Zhu C. A simple and efficient solar cell parameter extraction method from a single current-voltage curve. J Appl Phys 2011;110:064504–64507. http://dx.doi.org/10.1063/1.3632971.
[25] Peng L, Sun Y, Meng Z, Wang Y, Xu Y. A new method for determining the characteristics of solar cells. J Power Sources 2013;227:131–6. http://dx.doi.org/10.1016/j.jpowsour.2012.07.061.
[26] Cubas J, Pindado S, de Manuel C. Explicit expressions for solar panel equivalent circuit parameters based on analytical formulation and the Lambert W-function. Energies 2014;7:4098–115. http://dx.doi.org/10.3390/en7074098.
[27] Ghani F, Rosengarten G, Duke M, Carson JK. The numerical calculation of single-diode solar-cell modelling parameters. Renew Energy 2014;72:105–12. http://dx.doi.org/10.1016/j.renene.2014.06.035.
[28] Peng L, Sun Y, Meng Z. An improved model and parameters extraction for photovoltaic cells using only three state points at standard test condition. J Power Sources 2014;248:621–31. http://dx.doi.org/10.1016/j.jpowsour.2013.07.058.
[29] Nassar-eddine I, Obbadi A, Errami Y, El fajri A, Agunaou M. Parameter estimation of photovoltaic modules using iterative method and the Lambert W function: a comparative study. Energy Convers Manage 2016;119:37–48. http://dx.doi.org/10.1016/j.enconman.2016.04.030.
[30] Villalva MG, Gazoli JR, Filho ER. Comprehensive approach to modeling and simulation of photovoltaic arrays. IEEE Trans Power Electron 2009;24:1198–208. http://dx.doi.org/10.1109/TPEL.2009.2013862.
[31] Gao X, Yao C, Gao X, Yu Y. Accuracy comparison between implicit and explicit single-diode models of photovoltaic cells and modules. Acta Phys Sinica 2014;63:178401. http://dx.doi.org/10.7498/aps.63.178401.
[32] Li Y, Huang W, Huang H, Hewitt C, Chen Y, Fang G, et al. Evaluation of methods to extract parameters from current–voltage characteristics of solar cells. Sol Energy 2013;90:51–7. http://dx.doi.org/10.1016/j.solener.2012.12.005.
[33] Ortiz-Conde A, Lugo-Munoz D, Garcia-Sanchez FJ. An explicit multiexponential model as an alternative to traditional solar cell models with series and shunt resistances. IEEE J Photovoltaics 2012;2:261–8. http://dx.doi.org/10.1109/JPHOTOV.2012.2190265.
[34] Bendaoud R, Yadir S, Hajjaj C, Errami Y, Sahnoun S, Benhmida M, et al. Validation of a multi-exponential alternative model of solar cell and comparison to conventional double exponential model. In: 2015 27th international conference on microelectronics (ICM). p. 319–22. http://dx.doi.org/10.1109/ICM.2015.7438053.
[35] Lun S-X, Wang S, Yang G-H, Guo T-T. A new explicit double-diode modeling method based on Lambert W-function for photovoltaic arrays. Sol Energy 2015;116:69–82. http://dx.doi.org/10.1016/j.solener.2015.03.043.

[36] Ishaque K, Salam Z, Mekhilef S, Shamsudin A. Parameter extraction of solar photovoltaic modules using penalty-based differential evolution. Appl Energy 2012;99:297–308. http://dx.doi.org/10.1016/j.apenergy.2012.05.017.
[37] Jacob B, Balasubramanian K, Babu T S, Azharuddin SM, Rajasekar N. Solar PV modelling and parameter extraction using artificial immune system. Energy Procedia 2015;75:331–6. http://dx.doi.org/10.1016/j.egypro.2015.07.375.
[38] Muhsen DH, Ghazali AB, Khatib T, Abed IA. Parameters extraction of double diode photovoltaic module's model based on hybrid evolutionary algorithm. Energy Convers Manage 2015;105:552–61. http://dx.doi.org/10.1016/j.enconman.2015.08.023.
[39] Awadallah MA. Variations of the bacterial foraging algorithm for the extraction of PV module parameters from nameplate data. Energy Convers Manage 2016;113:312–20. http://dx.doi.org/10.1016/j.enconman.2016.01.071.
[40] Allam D, Yousri DA, Eteiba MB. Parameters extraction of the three diode model for the multi-crystalline solar cell/module using Moth-Flame Optimization Algorithm. Energy Convers Manage 2016;123:535–48. http://dx.doi.org/10.1016/j.enconman.2016.06.052.
[41] Chin VJ, Salam Z, Ishaque K. An accurate modelling of the two-diode model of PV module using a hybrid solution based on differential evolution. Energy Convers Manage 2016;124:42–50. http://dx.doi.org/10.1016/j.enconman.2016.06.076.
[42] Ismail MS, Moghavvemi M, Mahlia TMI. Characterization of PV panel and global optimization of its model parameters using genetic algorithm. Energy Convers Manage 2013;73:10–25. http://dx.doi.org/10.1016/j.enconman.2013.03.033.
[43] Easwarakhanthan T, Bottin J, Bouhouch I, Boutrit C. Nonlinear minimization algorithm for determining the solar cell parameters with microcomputers. Int J Sol Energy 1986;4:1–12. http://dx.doi.org/10.1080/01425918608909835.
[44] Shell SM55 module. <http://www.solar-bazaar.com/productis/Shell-SM55-Photovoltaic-Solar-Module.pdf>.
[45] KC200GT module. <http://www.kyocerasolar.com/assets/001/5195.pdf>.
[46] Characteristics of a PV module: Shell ST40. <http://www.physics.arizona.edu/~cronin/Solar/References/pvsyst%20outputs/st40%20a3.pdf>.
[47] Bühler AJ, Krenzinger A. Method for photovoltaic parameter extraction according to a modified double-diode model. Prog Photovoltaics Res Appl 2013;21:884–93. http://dx.doi.org/10.1002/pip.2170.
[48] Gong W, Cai Z. Parameter extraction of solar cell models using repaired adaptive differential evolution. Sol Energy 2013;94:209–20. http://dx.doi.org/10.1016/j.solener.2013.05.007.
[49] Guo L, Meng Z, Sun Y, Wang L. Parameter identification and sensitivity analysis of solar cell models with cat swarm optimization algorithm. Energy Convers Manage 2016;108:520–8. http://dx.doi.org/10.1016/j.enconman.2015.11.041.
[50] Askarzadeh A, Rezazadeh A. Extraction of maximum power point in solar cells using bird mating optimizer-based parameters identification approach. Sol Energy 2013;90:123–33. http://dx.doi.org/10.1016/j.solener.2013.01.010.
[51] Chen X, Yu K, Du W, Zhao W, Liu G. Parameters identification of solar cell models using generalized oppositional teaching learning based optimization. Energy 2016;99:170–80. http://dx.doi.org/10.1016/j.energy.2016.01.052.
[52] Askarzadeh A, Rezazadeh A. Artificial bee swarm optimization algorithm for parameters identification of solar cell models. Appl Energy 2013;102:943–9. http://dx.doi.org/10.1016/j.apenergy.2012.09.052.
[53] Askarzadeh A, Rezazadeh A. Parameter identification for solar cell models using harmony search-based algorithms. Sol Energy 2012;86:3241–9. http://dx.doi.org/10.1016/j.solener.2012.08.018.
[54] Niu Q, Zhang H, Li K. An improved TLBO with elite strategy for parameters identification of PEM fuel cell and solar cell models. Int J Hydrogen Energy 2014;39:3837–54. http://dx.doi.org/10.1016/j.ijhydene.2013.12.110.
[55] Niu Q, Zhang L, Li K. A biogeography-based optimization algorithm with mutation strategies for model parameter estimation of solar and fuel cells. Energy Convers Manage 2014;86:1173–85. http://dx.doi.org/10.1016/j.enconman.2014.06.026.
[56] Alam DF, Yousri DA, Eteiba MB. Flower pollination algorithm based solar PV parameter estimation. Energy Convers Manage 2015;101:410–22. http://dx.doi.org/10.1016/j.enconman.2015.05.074.
[57] Yuan X, Xiang Y, He Y. Parameter extraction of solar cell models using mutative-scale parallel chaos optimization algorithm. Sol Energy 2014;108:238–51. http://dx.doi.org/10.1016/j.solener.2014.07.013.
[58] Yuan X, He Y, Liu L. Parameter extraction of solar cell models using chaotic asexual reproduction optimization. Neural Comput Appl 2015;26:1227–39. http://dx.doi.org/10.1007/s00521-014-1795-6.
[59] Oliva D, Cuevas E, Pajares G. Parameter identification of solar cells using artificial bee colony optimization. Energy 2014;72:93–102. http://dx.doi.org/10.1016/j.energy.2014.05.011.
[60] Hachana O, Hemsas KE, Tina GM, Ventura C. Comparison of different metaheuristic algorithms for parameter identification of photovoltaic cell/module. J Renew Sustain Energy 2013;5:053122. http://dx.doi.org/10.1063/1.4822054.
[61] AlHajri MF, El-Naggar KM, AlRashidi MR, Al-Othman AK. Optimal extraction of solar cell parameters using pattern search. Renew Energy 2012;44:238–45. http://dx.doi.org/10.1016/j.renene.2012.01.082.
[62] El-Naggar KM, AlRashidi MR, AlHajri MF, Al-Othman AK. Simulated annealing algorithm for photovoltaic parameters identification. Sol Energy 2012;86:266–74. http://dx.doi.org/10.1016/j.solener.2011.09.032.
[63] Shell solar photovoltaic products. <http://www.efn-uk.org/l-street/renewables-lib/solar-reports/index_files/Shell-Solar.pdf>.
[64] PV model for thin film and other new technologies. <http://files.pvsyst.com/help/index.html>.
[65] Nelder-Mead algorithm. <http://www.scholarpedia.org/article/Nelder-Mead_algorithm>.
[66] Press WH, Teukolsky SA, Vetterling WT, Flannery BP. Numerical recipes: the art of scientific computing. 3rd ed. New York: Cambridge University Press; 2007.
[67] Bound constrained optimization using fminsearch. <http://www.mathworks.cn/matlabcentral/fileexchange/8277-fminsearchbnd-fminsearchcon>.
[68] Gao F, Han L. Implementing the Nelder-Mead simplex algorithm with adaptive parameters. Comput Optim Appl 2012;51:259–77. http://dx.doi.org/10.1007/s10589-010-9329-3.
[69] C++ implementation of the Lambert W(x) function. <https://github.com/DarkoVeberic/LambertW>.
[70] Veberič D. Lambert W function for applications in physics. Comput Phys Commun 2012;183:2622–8. http://dx.doi.org/10.1016/j.cpc.2012.07.008.